AD NUMBER

AD831048

NEW LIMITATION CHANGE

TO

Approved for public release, distribution unlimited

FROM

Distribution authorized to U.S. Gov't. agencies and their contractors; Administrative/Operational Use; Mar 1968. Other requests shall be referred to Air Force Flight Dynamics Lab. [FDFR], Wright-Patterson AFB, OH 45433.

AUTHORITY

AFFDL ltr dtd 1 Feb 1973

#831048#

THE PREDICTION OF MATERIAL TEMPERATURES ON WOVEN RETARDATION DEVICES

CHARLES J. SCOTT

UNIVERSITY OF MINNESOTA

TECHNICAL REPORT AFFDL-TR-67-170

MARCH 1968

This document is subject to special export controls and each transmittal tc foreign governments or foreign nationals may be made only with prior approval of the Air Force Flight Dynamics Laboratory.

AIR FORCE FLIGHT DYNAMICS LABORATORY
AIR FORCE SYSTEMS COMMAND
WRIGHT-PATTERSON AIR FORCE BASE, OHIO

NOTICE

ACCESSION for

CFSTI   WHITE SECTION
DOC   BUFF SECTION
UNANNOUNCED
JUSTIFICATION ....

....

BY
DISTRIBUTION/AVAILABILITY CODES

DIST.   AVAIL. and/or SPECIAL

100   prll 1968 - CO455 - 30-640

ABSTRACT

The primary purpose of this report is to present analytical tech-
niques for the prediction of instantaneous parachute temperatures for
any prescribed flight condition and history of operation. Sample calcu-
lations are presented which illustrate the technique by comparing measured
parachute temperature histories with several predictive techniques. A
variety of exact, transient heat conduction solutions are included (for
a cylindrical geometry) which cover a range of trajectory possibilities.
This was done because the transfer of heat to a conventional fabric or
coated-fabric parachute is governed primarily by the large resistance
to heat conduction into the interior. The commonly used infinite thermal
conductivity case is shown to produce surface temperatures which fall con-
siderably below the surface temperatures predicted by more exact (complete)
energy balances. For the extreme applied heat flux case (atmospheric en-
try), internal temperatures are accurately predicted by assuming the wall
temperature instantaneously assumes a steady state, radiation equilibrium
value ($q_w = 0$) and internal conduction governs the process. An approxi-
mate method is presented for the calculation of parachute fabric tempera-
tures when both the internal and external resistances to the flow of heat
are of importance. The results are compared with flight test data on a
full-scale parachute.

The distribution of this Abstract is unlimited.

iii

THE PREDICTION OF MATERIAL TEMPERATURES ON WOVEN RETARDATION DEVICES

CHARLES J. SCOTT

FOREWORD

This report summarizes the work done by the Heat Transfer Laboratory, Department of Mechanical Engineering, University of Minnesota, during a research program sponsored by the Recovery and Crew Station Branch of the Air Force Flight Dynamics Laboratory under Contract AF33615-67-1028, Project No. 6065, Task No. 606505. The manuscript was released by the author November 1967 for publication as a Technical Report. The contract's technical project monitor was C. A. Babish III of the Air Force Flight Dynamics Laboratory (FDFR). E. R. G. Eckert served as principal investigator of the contract at the University of Minnesota. The report covers work conducted from August 1966 through September 1967.

This technical report has been reviewed and is approved.

GEORGE A. SOLT, JR.
Chief, Recovery & Crew Station Branch
Vehicle Equipment Division
AF Flight Dynamics Laboratory

ii

TABLE OF CONTENTS

ILLUSTRATIONS

vii

SECTION I. INTRODUCTION

It is well known that by the aerodynamic heating effect vehicles flying at supersonic speeds are heated to such an extent that the skin temperatures and the temperatures inside the craft require the special attention of the designer. In addition, a growing interest in aircraft vehicle recovery operations has directed attention to a variety of deceleration devices. In many cases a sizeable portion of the initial kinetic energy of the primary or forebody is converted into an increase in internal energy of the retardation device--and the aerodynamic heat transfer of the deceleration device becomes a design factor.

Aerodynamic decelerators must possess a large drag-to-weight ratio and normally must be capable of being stored in a small volume. Therefore, most drag-producing devices are relatively thin and flexible. Towed decelerators such as ribbon or hyperflo parachutes, balloons, ballutes, etc., have flexible canopies. Other proposals incorporate structural members (cones or paragliders) or hybrid systems such as the AVCO drag brake (1)* and the NASA rotornet (2).

Impermeable retardation devices are aerodynamically unstable when utilized in a supersonic flow. As a result, nearly all the retardation devices discussed above employ extended porous surfaces 'n conjunction with other venting techniques (see Figure 1). Most conventional textile fibers either melt or are seriously degraded by exposure to temperatures above 500°F. It is desirable to replace these fibers with materials of higher

---

*Numbers enclosed by parentheses refer to references.

Figure .. Ochute nd.ris..riod
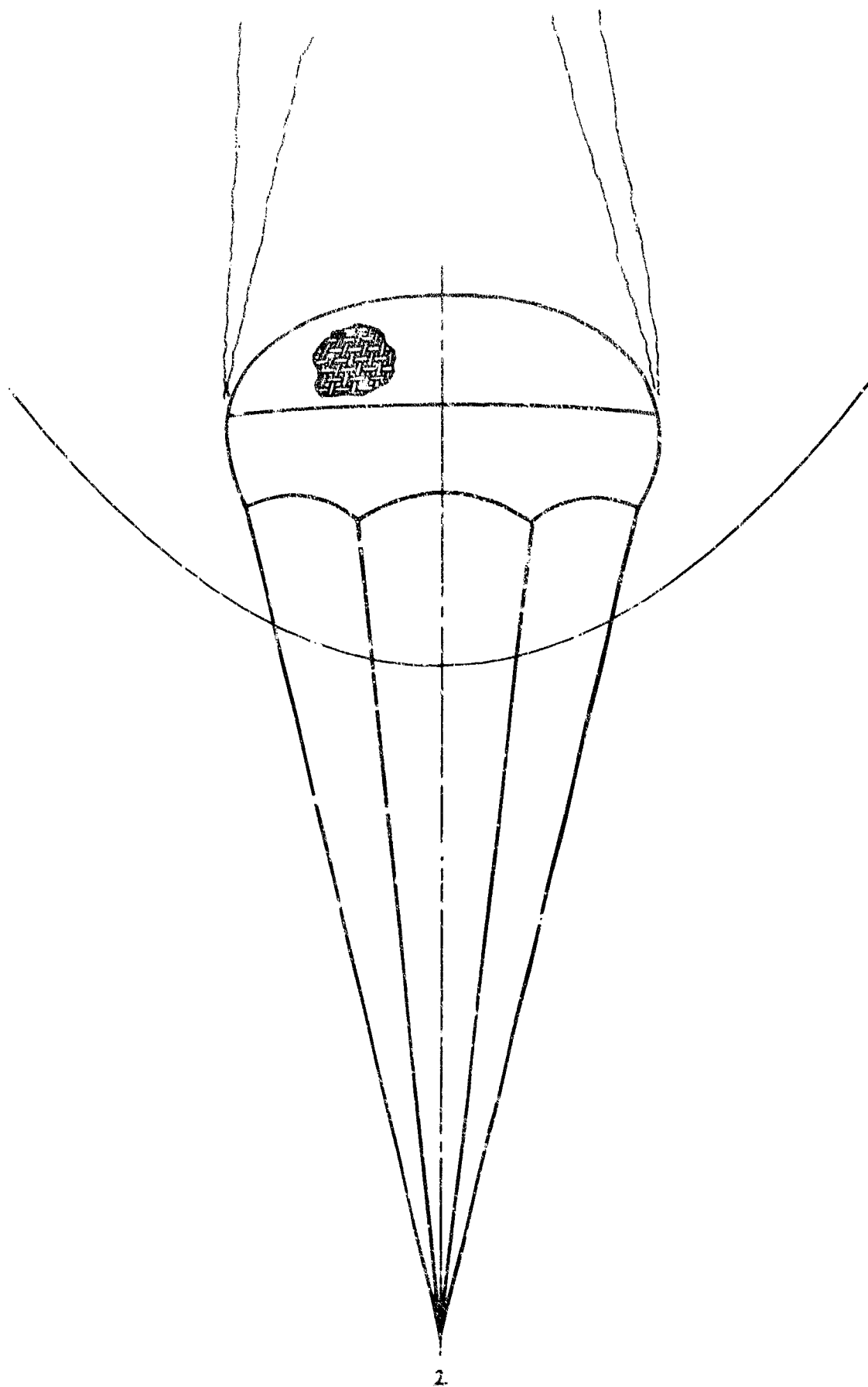
thermal durability such as fine metallic wires in which operational temperatures are close to 2000°F.

It is felt that for the purpose of analysis the flow field associated with a porous retardation device includes large-scale phenomena enveloping the entire device and small-scale processes associated with the local flow about a single element in the mesh material itself. The large-scale phenomena, such as parachute shape or size and the velocity and altitude, involve the external aerodynamics of the problem and contribute the end or boundary conditions (such as pressure ratio or Reynolds number) to the small-scale phenomena.

The mesh element geometry under consideration is a porous weave consisting of individual round wire filaments. Wind tunnel (3) and free-flight tests (4) of ribbon parachutes have shown considerable degradation of performance due to the high heat transfer coefficients near the edges. Lately wind tunnel tests of small models have indicated that reasonable inflation and attitude stability may be attained with a fine-mesh roof material (5). The flow through a single pore is taken to be analogous to the flow through a nozzle. At supersonic flight speeds and at very high porosities* discrete shock waves form ahead of each cylinder. If the porosity is lower, i.e., insufficient to permit supersonic flow to be "started" in each nozzle in a manner similar to the

---

*Porosity is defined geometrically as the ratio of open area to total area of the forward-facing surface of the retardation device.

starting process in a closed-channel wind tunnel, a continuous shock appears ahead of the entire mesh surface. At such intermediate porosities and sufficiently large Reynolds numbers, a discrete boundary layer will form on each cylinder. Only at very low porosities and Reynolds numbers will the individual boundary layers merge to completely fill the pores and establish a continuous boundary layer over the entire mesh surface. Only the intermediate porosity-discrete boundary layer case will be studied in this report.

Large-Scale Phenomena

The range of interest in the present study consists of altitudes from sea level up to 200,000 feet and flight Mach numbers ranging from 3 to 6. A typical "problem" might be Mach 5 operation above 70,000 feet with a nominal parachute diameter of 2 to 10 feet and geometric porosities of 25%. A concave hemisphere canopy is a typical shape considered for supersonic operations although specification of the exact geometry is not necessary. In previous work (6), it was felt that a good starting point for study of the large-scale phenomena was the simple concave hemisphere. The experimental results of Reference 6 indicate that at angular locations up to 75 degrees from the stagnation point, the static pressure on the upstream surface of the concave hemisphere is equal to the total pressure. This means that there is practically no flow near and parallel to the surface of the hemisphere except near the edge. Of course, in supersonic flow, a

4

nearly normal shock would stand ahead of the hemisphere and this would
produce a completely subsonic flow regime inside of the concave hemisphere.[+]
In the absence of any parachute porosity, the pressure on the upstream
side of the chute is closely approximated by the total pressure behind the
normal shock. In determining the pressure on the rearward (downstream) face
of the parachute, we are led to a base pressure phenomenon described by
H. H. Korst (7).

The discussion in the previous paragraph illustrates a technique for
computing the pressures and hence the pressure ratio across a chute with
no porosity. The analysis for the base pressure problem has been extended
to the case of flow through the chute with small momentum only. Since
this last condition is rarely met in the case of practical parachute
configurations, the pressure ratio across the chute openings must be
found from experiment.

Small-Scale Phenomena

A high-temperature, high-density flow is produced inside the canopy.
This flow passes through the individual openings of the mesh. Heat is
transferred from the hot gases to the mesh elements. Therefore, it is

---

[+]Schlieren photographs of supersonic wind tunnel tests indicate
that the normal shock one anticipates ahead of a low-porosity blunt cano-
py is altered into a conical shape by the viscous forebody wake. Mainly
the low energy portions pass through the canopy.

5

the distribution of heat flux to the surfaces of a crossed mesh which is of primary importance. The typical element may be considered as a cylinder aligned normal to the flow. The element is bounded on each side by an opening (slot) through which the oncoming flow passes. The approaching flow may or may not separate upstream of the cylinder. This process has not been clearly defined.

The flow passing through the slots exhibits properties which depend upon the overall applied pressure ratio. In most flight applications, the applied pressure ratio will be such that the flow in the slot may be sonic. Additional energy is available for further expansion of the stream as it emerges from the slot such that localized regions of supersonic flow will occur downstream of the slot. Between the supersonic jets emerging from the slot and the rearward-facing surface of the cylinder, two regions are found. The first is a conventional free-shear layer in which the streamwise component of velocity diminishes from the value found in the jet to a near-zero condition. Adjacent to the shear layer there exists a small region of reverse flow with a circulating vortex. The local pressure in the separation bubble is determined by local base pressure phenomena (the flow issuing from the slot). The mean near-wake pressure which exists further donwstream is determined by the gross geometry and the freestream Mach number. These two pressures are generally not equal. Therefore, further recompression exists downstream of the jets issuing from the individual slots. The local base pressure behind an individual ribbon is therefore determined by the slot pressure ratio and the recompression process in the jets.

6

Flow Field Analysis

On the basis of the preceding discussion, the following assumptions were made regarding the flow field about the parachute:

1) No consideration is given to the presence of the forebody wake and to corresponding modifications of the canopy shock wave. The local flow parameters (M_1, p_1, T_1, ρ_1) ahead of the body (station 1) are determined solely by the trajectory.

2) A detached shock stands in front of the inlet area A_2 (see Figure 2). The shock is assumed to be a normal shock. The shock is not influenced by the riser lines. The fluid properties downstream of the shock (station 2) are determined by the normal shock relations.

3) The flow through the skirt is one-dimensional. The local flow parameters are determined using a steady, one-dimensional, isentropic, compressible flow.

4) The local flow through the roof is analogous to the flow in the sonic throats of a multinozzle grid. The sonic pressure in the mesh minimum area is found from the isentropic expansion from the fictitious reservoir (Figure 3) with conditions (p_0', T_0) that exist behind the shock. Continuity of mass flow through the inlet and throat can be used to determine the approach flow velocity inside the roof at station 3.

5) This approach to calculating the heat flux rates to porous retardation devices is also subject to the following limitations:

    a) porosities such that individual boundary layers exist on each filament and

    b) continuum boundary layer concepts on each filament.

<center>7</center>
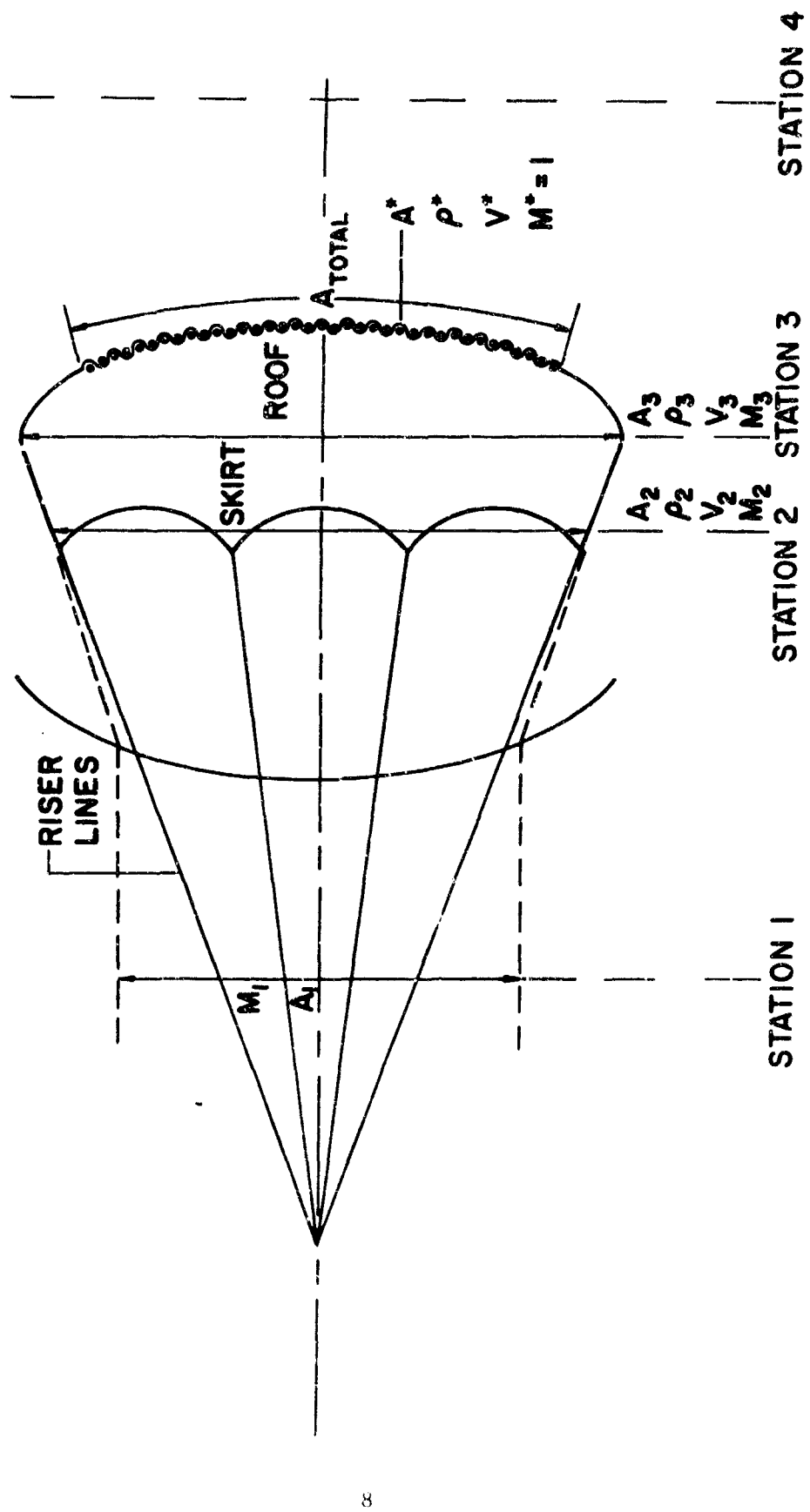
Figure 2. Parachute Flow Field

P_o' T_o ρ_o'

FICTITIOUS
STAGNATION
CONDITIONS

A_2
M_2
ρ_2
V_2

A^*
ρ^*
V^*
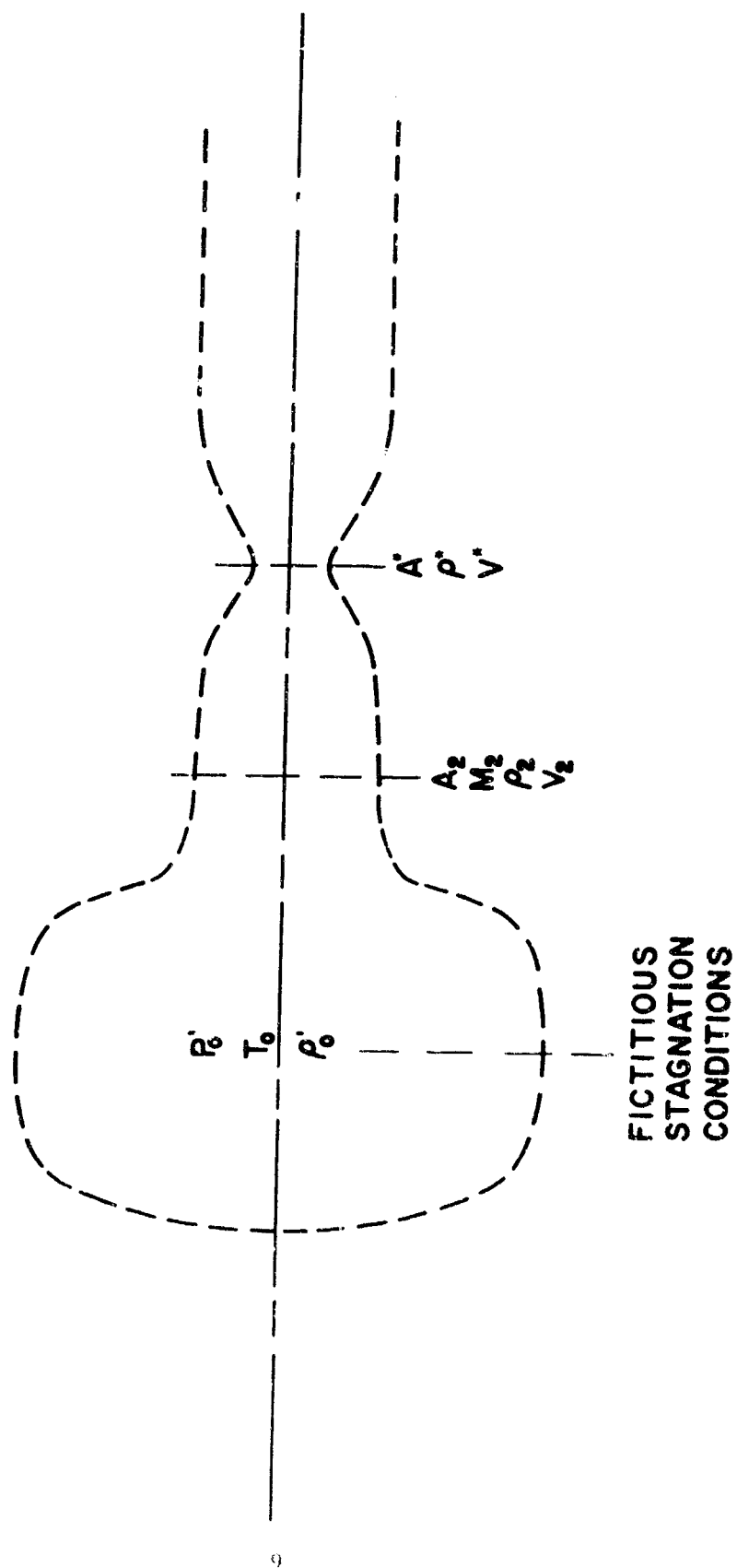
Figure 2. Trajectory Nomenclature

9

Heat Transfer Phenomena

Most parachutes are constructed of fabrics which are very poor
thermal conductors. Examination of parachute canopies after experimental
tests has revealed the importance of parachute material mass and its
distribution. Areas remote from overlapped seams have obtained higher
temperatures than in the higher mass seam areas. The thermal heat sink
of a given component is significant in determining the final temperature
attained by that component.

When the decelerator is being heated, the maximum temperature the
surface can attain is the equilibrium temperature--i.e., the temperature
resulting from a balance between convective heating and radiation cooling.
Therefore the maximum temperature which may develop is strongly dependent
on the film heat transfer coefficient and the emittance of the material.
The radiation equilibrium temperature closely approaches the adiabatic
wall temperature at low Mach numbers where the total temperature is small.
The departure is significant above Mach number 2.0 due to the T^4 variation.

For the "actual" or "instantaneous" temperature, the local heat transfer
coefficient, the surface emittance, and the thermal diffusivity of the
decelerator material must be known for each point of the trajectory. Fre-
quently time-temperature histories are computed using the assumption of
infinite object thermal conductivity coupled to the heat sink ability of
the parachute. Calculated maximum temperatures involve a balance between
convective heat input and radiative heat loss and do not include heat
storage terms. The zero convective heat flux wall temperature--referred
to as the recovery or adiabatic wall temperature, T_{aw}, results in wall

temperatures which are close to the freestream total temperatures since the expression for T_{aw} is

$$\frac{T_{aw}}{T_{0_\infty}} = \frac{1 + r\ (\frac{\gamma - 1}{2})\ M_\infty^2}{1 + (\frac{\gamma - 1}{2})\ M_\infty^2} \tag{1}$$

and the values of r fall in the range

$$0.85 \simeq (Pr)^{1/2} = r_{lam} \leq r \leq r_{turb} = (Pr)^{1/3} \simeq 0.90 \tag{2}$$

Some authors have recommended porous drag devices because of the advantages offered from the points of view of flexibility, packaging, manufacture, and aerodynamic stability. There is a serious disadvantage of increased heat transfer from the surrounding air to the porous retardation device. When the retardation device is made up of a porous weave consisting of round filaments, and the porosity of the weave is such that a single normal shock forms ahead of the body, the total heat transfer to such a woven cloth is equal to the sum of the heat transfers to the individual filaments. It is a well-established fact that the stagnation point heating rates vary as the inverse square root of the element radius. Therefore the ratio of the heating rates of porous materials to solid materials is equal to the square root of the nose radius to filament radius. For example, a weave consisting of 0.010-inch-diameter filaments-50 to the inch (25 percent geometric porosity), receives 50 times as much heat per unit area as a solid material of 1 foot radius under the same approach flow conditions. The area available for heat transfer is also increased.

11

The equilibrium temperature is affected to a lesser amount because woven materials have higher emissivities than solid surfaces of the same parent material—a geometrical result due to the great number of cavities. These cavities tend to alter the reflection characteristics and therfore to increase the absorptivity above that of a solid surface. At equilib rium, the emissivity and absorptivity are equal and increased emissivity results.

Mass Transfer Cooling Effects

At the present time useful metallic and ceramic fibers are still in the developmental stage and parachute materials can only be used below their softening temperature (for nylon 350°F). This limitation suggests the use of non-permanent coatings that sublime or ablate. In consideration of high-temperature materials for parachute application, coated fabrics or coated fibers are useful. The short aerodynamic heating periods associated with first-stage decelerators permit the use of ablative-type insulating coatings of conventional internal fibers (nylon and Nomex). For orbital re-entry trajectories coated metal fiber fabrics would be effective. It has been demonstrated (8) that subliming coatings do substantially increase the operating lifetime of the base material. The increased thermal protection results primarily from the added mass (heat sink effect). The extreme mechanical environment (parachute opening shock, flutter, etc.) is extremely detrimental to the bond between the coating and parent material such that frequently the coating material is removed by mechanical rather than thermal causes.

Trajectory Heat Transfer Considerations

The greatest source of uncertainty in engineering calculations of the energy exchange process to the mesh elements lies in the determination of the convective heat flux as characterized by a heat transfer parameter Nu which is a function of a number of parameters. This is expressed by the following dimensionless relationship

$$Nu = f(Re, M_1, Kn, T_w/T_0, geometry). \qquad (3)$$

The Reynolds number Re describing the flow conditions around the fibers will, in this report, be based on cylinder diameter D and on the average velocity and properties in the flow through the slots between the mesh elements where, for supercritical pressure ratio, sonic velocity exists. This Reynolds number is denoted as $Re^* = \frac{\rho^* a^* D}{\mu^*}$. In Figure 4, Re^*/D is plotted versus descent Mach number M_1 for altitudes ranging from sea level to 200,000 feet. This Reynolds number is presented since it does not require the specification of a body dimension which varies with a specific parachute. The large values of Re^*/D which ex low altitudes produce high heat flux rates. The short-dashed curve is a curve of constant dynamic pressure (connected with the descent velocity) of 1 lb. per square foot--below which reliable self-inflation of flexible drag devices cannot be expected. The curve labeled "stagnation temperature = 1000°F" illustrates the heat transfer problem as determined by Mach number effects. The operating regime of conventional parachutes lies within the envelope of the two preceding curves.
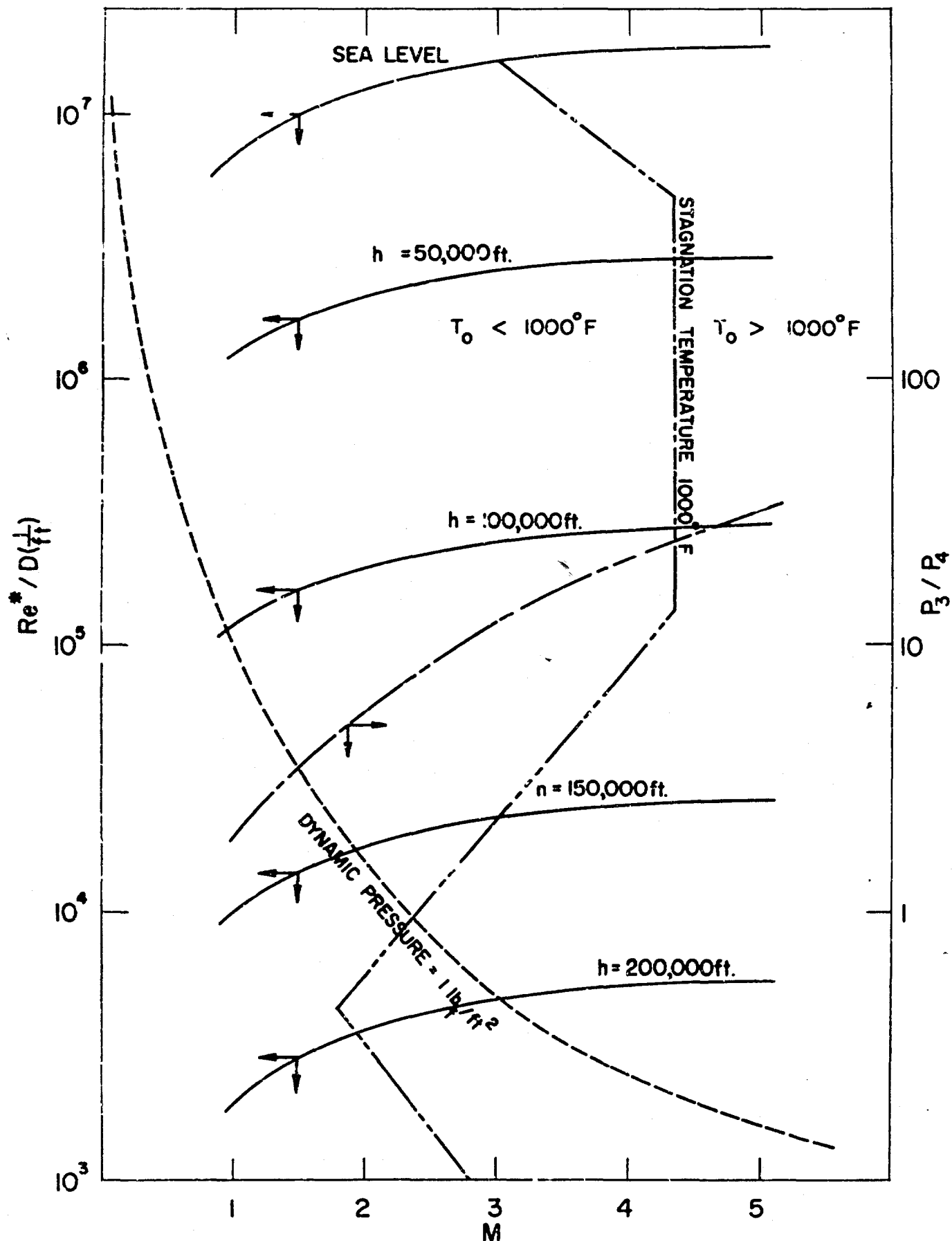
Figure 4. Unit Reynolds Number Versus Flight Mach Number for Various Flight Altitudes

14

The descent Mach number M_1 has only an indirect influence upon the heat transfer to the mesh elements insofar as it determines the pressure and temperature both inside the canopy and behind it. For the flow and heat transfer around the ribbons, the pressure ratio p_3/p_4 is a more suitable parameter. Its use has the further advantage that it can be readily measured in a wind tunnel experiment on a parachute model. The pressure ratio curve presented in Figure 4 is the ratio of the total pressure behind a normal shock to the freestream static pressure and represents the minimum pressure ratio which should be studied at any simulated flight Mach number.

The Prandtl number Pr, whose value is approximately 0.7 under normal atmospheric conditions, deviates up to $\pm$ 10 percent from this value up to temperatures of approximately $6,000°R$. At altitudes up to 400,000 feet the stagnation temperatures for Ma $\leq$ 10 will be below $6,000°R$. The deviation of the Prandtl number from the value 0.7 will be neglected.

The Knudsen number Kn will enter as a parameter only at very low densities. It can be expressed as a relation between Mach number and Reynolds number, for instance by $\frac{M_1}{\sqrt{Re}}$. In this expression the mean free path of the molecules is related to the boundary layer thickness. The determination of the critical value of $\frac{M_1}{\sqrt{Re}}$ depends upon the shape of the body which affects the boundary layer growth. However, for an approximate evaluation it seems justified to introduce M* and Re* as characteristic values in the Knudsen number. Hermann (9) gives as critical value $\frac{M^*}{Re} = 10^{-3}$. In the present case, $M^* = 1$. Thus, continuum flow can be expected to exist for descent conditions at which

15

Re* > 1000. The conditions for which this is the case are evident from Figure 4. The results presented in this report are valid for the continuum flow regime. Summarizing the foregoing discussion on the influence of the various parameters upon the heat transfer on a parachute fiber, we can expect a relation

$$Nu = f(Re^*, \frac{p_3}{p_4}).$$

$$(4)$$

This relation, then, has to be determined by experiments.

As mentioned above, it is convenient to define a Reynold's number based on the velocity and flow properties in the sonic orifice and the slot width

$$Re^*_D = \frac{\rho^* a^* D}{\mu^*}$$

$$(5)$$

In the flight case the static temperature T_1 and pressure p_1 are determined by the flight altitude. A total pressure p_0 and temperature T_0 are determined once the flight Mach number is prescribed. Since the bow shock is assumed to be normal, the total pressure p'_0 (inside the canopy) is determined from p_0 and M_1. The total density behind the bow shock, is computed from p'_0, T_0 and the proper equation of state. Finally, the sonic density and speed are determined from an isentropic expansion from p'_0, T_0, to p^* and T^*. The viscosity μ^* is a known function of the temperature T^*.

Once a method for calculating the heat transfer coefficient is selected, an appropriate heat balance solution must be applied. Either of two approximate procedures can be used, as follows:

16

1.   <u>One-dimensional transient solution:</u>

Consider the fabric wall as a cylinder exposed to aerodynamic heating on the surface. A heat balance then can be written for the conditions at the outer surface. The condition for heat input at the outer surface by convection alone from a fluid at an adiabatic wall temperature (T_{aw}) is

$$h(\tau) \; [T_{aw} - T(r,\tau)] = - k \left[\frac{\partial}{\partial r} T(r,\tau)\right] \tag{6}$$

This equation implies that the element is subjected to a uniform thermal environment around its periphery. Thus, one can approximate the heating of the roof panel element by a cylinder subject to a constant temperature environment at the instant of time under consideration. As a first approximation, the radiation away from the outer surface is neglected but can be included if necessary as surface temperatures reach values where they become an important factor. The rate of heat conduction into the cylinder then can be calculated in conjunction with one of the suggested methods for calculating the heat transfer coefficient, by iteration over a finite time interval. This equation is solved over the critical deceleration time with aid of a computer, or it is estimated by using thermal-response charts such as those available in Section IV, Case C. This transient type of heat balance solution is useful particularly in situations where the deceleration takes place over a short time interval.

17

2.   Heat balance solution:

Consider the fabric wall as a cylinder exposed to aerodynamic
heating on its external surface which behaves like a heat sink
with practically no temperature gradient through its thickness.
Then, the following heat balance can be written:

$$hS_1 \ (T_{aw} - T_w) \ - \ \sigma S_3 \varepsilon T_w^4 \ = \ \rho_m V_m c_{p_m} \frac{d\overline{T}}{d\tau} \tag{7}$$

This heat balance, developed in Section I, is written at the
outer surface on the assumption that there is no internal ra-
diation-energy interchange. This equation, combined with the
method selected for calculating the heat transfer coefficient,
can then be solved by iteration, by assuming various wall
temperatures for the instant of time under consideration until
a balance is achieved (i.e., a quasi-steady-state condition
is reached along the trajectory path for a finite time interval).
This heat balance solution is useful particularly in situations
where the material has practically no temperature gradient with-
in it (Newtonian heating). Thus, a simple estimate of the sur-
face-temperature rise can be made if one assumes that such a
temperature gradient does not exist.

Either Equation (6) or (7) may be used to estimate the maximum
temperature the parachute may attain during the heating process. This
equilibrium temperature will normally exceed the actual surface tempera-
ture during the parachute heating cycle. There are cases, such as atmos-

18

pheric entry, in which the instantaneous equilibrium temperature looks
like one-half a cycle of a sine wave. The complete solution of Equation
(7) which incorporates the internal heat sink effect, leads to actual
wall temperatures which, at times, exceed the equilibrium temperature as
sketched below:
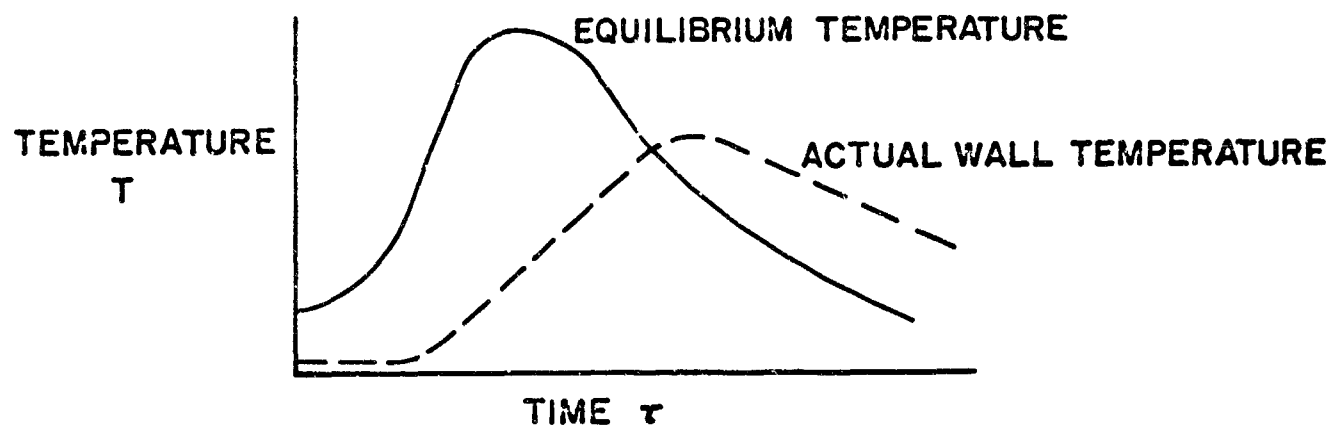
The methods described above must be modified if the decelerator
reaches its charring temperature or melting temperature before attaining
the equilibrium temperature. Certainly computed temperatures that are in
excess of the melting temperatures have no physical significance. When
the surface temperature reaches the melting temperature the problem
shifts to a transient heat conduction problem with a constant surface
temperature.

19

SECTION II.   EXTERNAL ENERGY TRANSFER

Energy Balance

The time-temperature history of a deceleration device is governed
by the principle of energy conservation which is expressed by the relation
between energy flow rates $\dot{Q}$ as

$$\dot{Q}_{entering} - \dot{Q}_{leaving} = \dot{Q}_{stored} \qquad (8)$$

In the case of a deceleration device moving through the atmosphere the
following energy flows appear:

1) Energy flow into the parachute by convection, $\dot{Q}_c$

2) Energy gain due to incident solar radiation, $\dot{Q}_{r_{so}}$

3) Energy loss from the parachute by radiation to space, $\dot{Q}_{r_{sp}}$

4) Energy loss due to radiation to the earth, $\dot{Q}_{r_e}$

5) Energy stored by the parachute, $\dot{Q}_{st}$

These terms will be discussed in the following paragraphs.

1) <u>The heat transfer into the parachute by convection</u>, $\dot{Q}_c$, is cal-
culated from the relation

$$\dot{Q}_c = hS_1 \ (T_{aw} - T_w) \qquad (9)$$

where

S_1 = total surface area of decelerator exposed to convective
   heating, (ft^2)

h = convective heat transfer coefficient, $(BTU/ft^2\text{-sec-}°R)$

T_{aw} = adiabatic wall temperature, (°R)

T_w = temperature of the surface of the decelerator, (°R)

The flat plate with constant wall temperature serves as the standard condition to which simple formulae apply. For this case the differential equations which describe the flow and energy conditions are well-established for a laminar boundary layer at normal conditions of pressure (continuum flow regime) and temperature (ideal gas behavior). The principal difficulties in solving these equations stem from the large variations with temperature and pressure of such thermal properties as viscosity, thermal conductivity, density, and specific heats. Experimental imperfections generally lead the designer to conclude that in the laminar range, the most reliable information is obtained from analytical calculations. If the geometry is complex and/or transition to turbulent flow takes place on the body, then empirical methods must be resorted to. The proposed methods for the calculation of h are summarized in Section II.

2) <u>The energy gained due to incident solar radiation</u> may be determined from the relation

$$\dot{Q}_{r_{so}} = I\alpha S_{rad} \tag{10}$$

where

I = solar radiation intensity; a reasonable estimate of its value is 425 BTU/ft^2-hr

α = absorptivity for solar radiation of the parachute material; a typical value is 0.2

S_{rad} = projected surface area of body, (ft^2)

21

3) The energy loss from a parachute by radiation to space is given by

$$\dot{Q}_{r_{sp}} = \sigma S_{rad} \, \varepsilon \, F_{p-sp} \, (T_w^4 - T_{space}^4) \tag{11}$$

where

σ = Boltzmann constant equal to 0.173×10^{-8} BTU/ft^2-hr-$^\circ$R^4

F_{p-sp} = radiation shape factor between parachute and space

ε = emissivity of the parachute material for long wavelength radiation; a typical value is 0.8

T_w = temperature of the walls, ($^\circ$R)

T_{space} = temperature of space, (7°R)

4) The energy loss from the parachute to the earth is given by the relation

$$\dot{Q}_{r_e} = \sigma F_4 S_{rad} \, \varepsilon \, F_{p-earth} \, (T_w^4 - T_{earth}^4) \tag{12}$$

where

$F_{p-earth}$ = radiation shape factor between the parachute and the earth

ε = emissivity; has the same significance and practically the same value as in Equation (11)

T_{earth} = average earth temperature; assumed to be 520°R

5) The rate at which energy is stored by the parachute is given by the relation

$$\dot{Q}_{st} = \rho_m V_m c_{p_m} \frac{d\overline{T}}{d\tau} \tag{13}$$

22

where

ρ_m = average density of parachute material (lbm/ft^3)

V_m = total volume of parachute material (ft^3)

c_{p_m} = heat capacity of parachute material ($BTU/lbm-°R$)

$\frac{d\overline{T}}{d\tau}$ = time rate of change of the average temperature f the parachute mass, ($°R/hr$)

Total Energy Balance

An energy balance may now be written based on the above equations to yield

$$hS_1(T_{aw} - T_w) + I\alpha S_2 - \sigma S_3 \epsilon (T_w^4 - T_{space}^4) +$$

$$\sigma F_4 S_4 \, \epsilon (T_w^4 - T_{earth}^4) = \rho_m V_m c_{p_m} \frac{d\overline{T}}{d\tau} \tag{14}$$

In a majority of cases considered the terms for the energy flow into the parachute by solar radiation and for energy loss due to radiation to the earth are generally negligible compared to those of radiation to space. In addition the temperature of space ($T_{space} = 7°R$) may also be neglected compared to equilibrium temperatures of practical interest. Finally, if no heat is absorbed by the parachute the convective flux must be equal to the radiant flux. This condition permits a simple determination of the equilibrium surface temperature T_e. Consequently

$$hS_1 \, (T_{aw} - T_e) = \sigma S_3 \epsilon T_e^4 \tag{15}$$

23

or rewritten as

$$\frac{T_e^4}{T_{aw} - T_e} = \frac{h}{\sigma \epsilon} \left(\frac{S_1}{S_3} \right) \tag{16}$$

Equation (16) may be solved for the equilibrium temperature in the above form by trial and error, or the following system may be used which is an explicit solution for T_e from Equation (16):

$$T_e = \frac{1}{2} \left[-\sqrt{L} + \sqrt{L - 2(L - m/\sqrt{L})} \right] \tag{17}$$

where

$$L = \left[\frac{m^2}{2} + \sqrt{\frac{m^4}{4} + \frac{64n^3}{27}} \right]^{1/3} + \left[\frac{m^2}{2} - \sqrt{\frac{m^4}{4} + \frac{64n^3}{27}} \right]^{1/3} \tag{18}$$

$$m = \frac{h}{\sigma \epsilon} \left(\frac{S_1}{S_3} \right) \qquad , \qquad n = \frac{h}{\sigma \epsilon} \left(\frac{S_1}{S_3} \right) T_{aw} \tag{19}$$

Opening Period

The extremely short time to maximum temperature of some parachutes should be noted since it becomes of the same order of magnitude as the opening time (which falls in the range of 1/20 to 1/2 second, depending on the parachute design). It is estimated in Reference 10 that the time to maximum temperature should be at least ten times greater than the parachute opening time before the opening effect can be neglected.

The greatest source of uncertainty in Equation (16) lies in the evaluation of h. It has been demonstrated that the dimensionless heat transfer coefficient (the Nusselt number) for the constant property, incompressible flow case may be utilized to calculate heat transfer for

24

the variable property, supersonic case if the various physical properties which appear are evaluated at a reference temperature T_r. According to Reference 11,

$$T_r = T_\delta + 0.5(T_w - T_\delta) + 0.22(T_{aw} - T_\delta) \tag{20}$$

The recovery temperature is dependent on the trajectory and will vary with altitude. At a given altitude the recovery temperature is that temperature which a parachute would ultimately assume under the sole influence of steady state convective heat transfer, i.e., in the absence of other modes of heat transfer. The recovery temperature is determined by the extent the kinetic energy of the air stream is converted into thermal energy. For blunt shapes, the conversion is very nearly complete such that the recovery temperature is closely equal to the stagnation temperature.

According to Equation (20), the calculation of the reference temperature (T_r) requires advance knowledge of the unknown wall temperature. For blunt bodies, normally $T_\delta \approx T_{aw} >> T_w$ and $T_r = 1/2 (T_0)$ such that the reference temperature T_r is insensitive to T_w for the early portion of the trajectory.

25

SECTION III. CONVECTIVE HEAT TRANSFER COEFFICIENT

In the selection of the film heat transfer coefficient it is necessary
to determine the characteristics of the viscous flow field adjacent to
the surface elements of the decelerator. There are no exact calcula-
tions of "supercritical woven mesh flow" so that a rigorous development
is not possible. There have been two analytical models proposed for the
prediction of the average convective heat transfer coefficient for mesh
flows of intermediate porosity (single bow shock--individual boundary
layers on each filament). They are as follows:

1) two-dimensional laminar stagnation flow coupled with stagnation
   point velocity gradients for low speed, potential flow over an
   infinite cylinder

and

2) axisymmetric turbulent boundary layer flow as applied to the
   throat region of a supersonic nozzle

Rose, Probstein, and Adams (12) have reported that the critical
Reynolds number for the transition from a laminar to a turbulent boundary
layer is approximately 4×10^5, based on conditions at the outer edge
of the boundary layer.[+] With fiber diameters on the order of 0.004 - 0.050
inch, Figure 6 reveals that a laminar boundary layer will exist over the

---

[+]A somewhat more exact and complex criterion for transition is that
of an empirically determined critical Reynolds number based not on the
wetted length but on the momentum thickness. The critical momentum thick-
ness Reynolds number is approximately 250 (13).

entire front face of a typical mesh element for all Mach numbers and altitudes under consideration for woven mesh parachutes.

The experimental results of Scott and Ruiz-Urbieta (14; Figures 5-8) produced an engineering conclusion that there are no large variations of local heat flux around the periphery of a woven mesh surface and that the conventional laminar stagnation point prediction is a useful first approximation. In this paper, local measurements were made on an enlarged woven mesh in which the individual fibers were one inch in diameter. Measurements of the local pressures (Figure 6), recovery temperatures (Figure 7), and convective heat transfer coefficients (Figure 8) were made on the forward and rearward surfaces of the mesh at locations indicated in Figure 5. Pressure ratios across the mesh were varied from subcritical, through the critical, and into the supercritical regime. Comparisons of the experimental data with the two proposed methods of calculating average heat transfer coefficients are readily observed. It is of importance that no large variations of h appear—a result which justifies the use of a single heat transfer coefficient applied to the entire surface. It is of interest here that the experiments revealed that regions of separated flow covered approximately 70 percent of the surface area exposed to convective heating. Secondly, comparisons of the data with both predictive models mentioned above revealed that while the two methods were generally conservative, some of the data taken at locations between the stagnation line and the sonic throat, do fall above the stagnation point predictions. Since the experimental model was

27
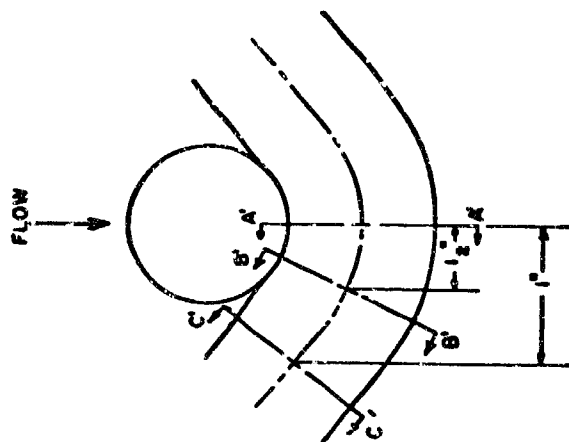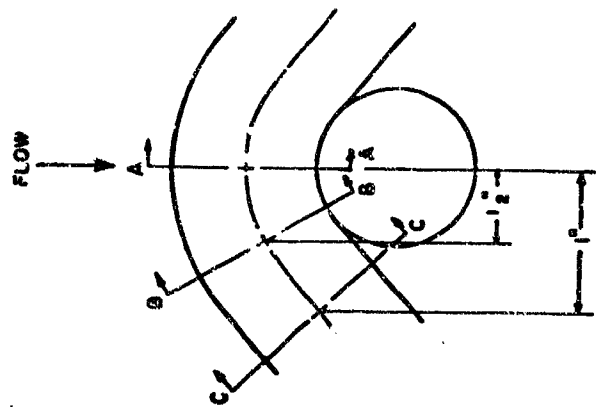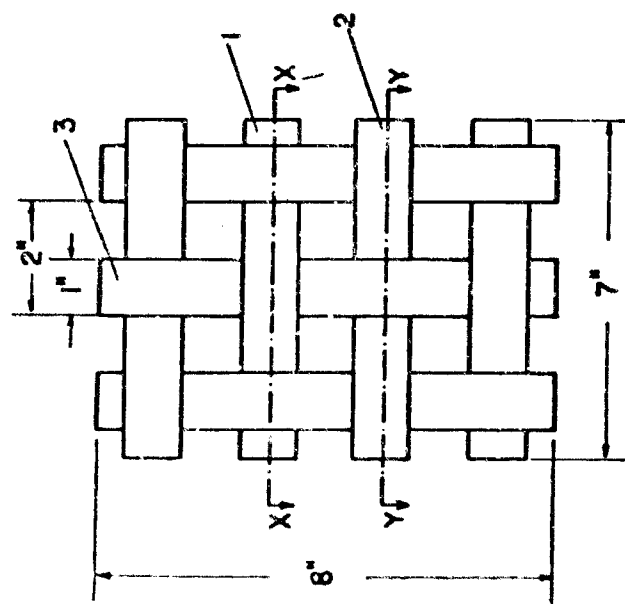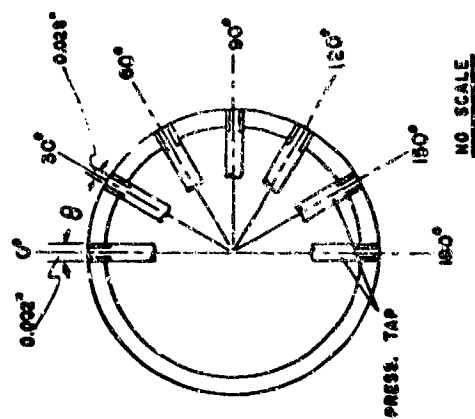
Figure 5. Experimental Notation
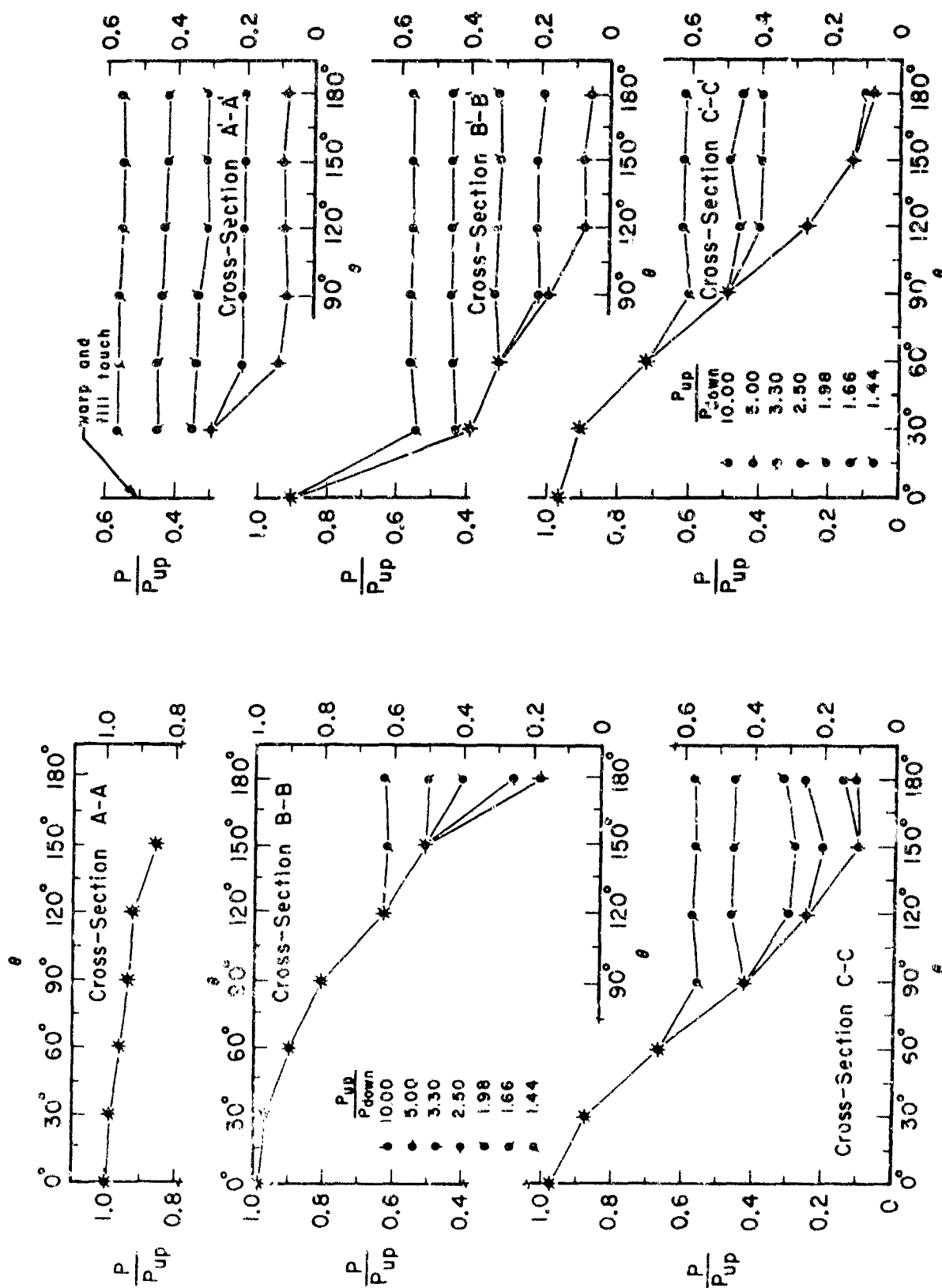
Figure 5. Pressure Distributions on Individual Mesh Elements
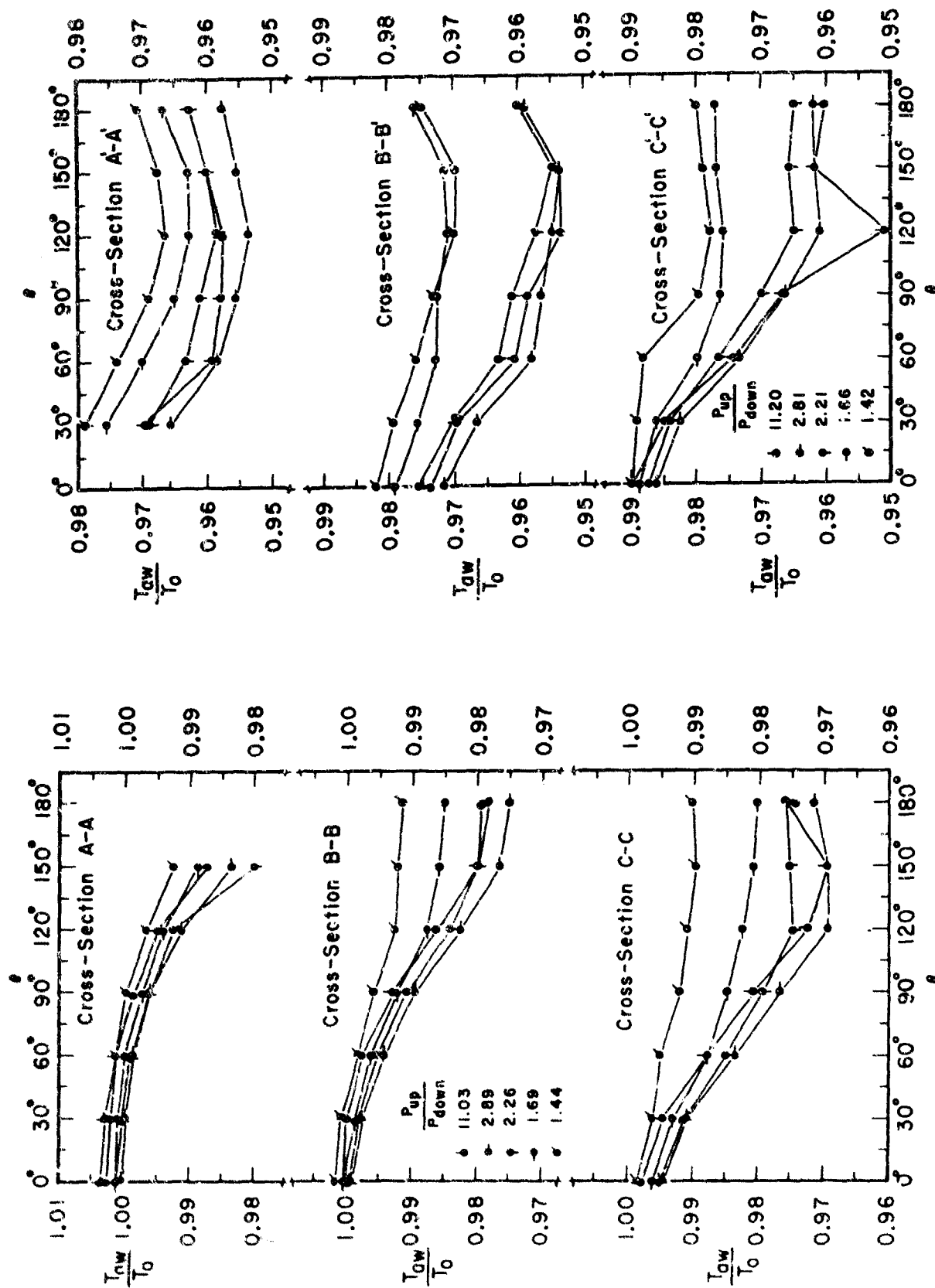
Figure 7. Recovery Temperature Measurements on Mesh Elements
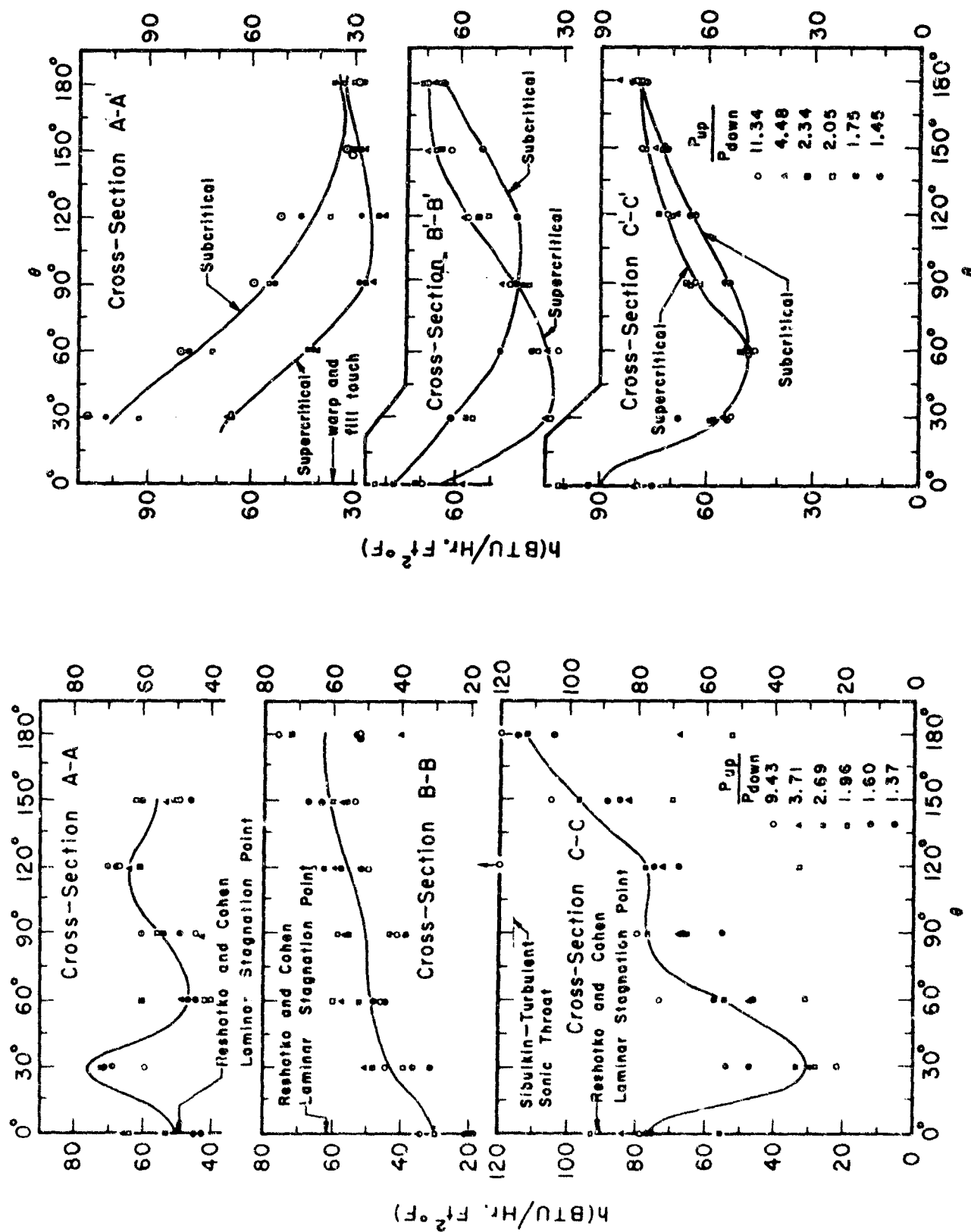
Figure 8. Heat Transfer Coefficients on Mesh Elements and Comparisons with Analyses

hollow and of thin-walled construction, internal heat conduction could not damp out these local variations--as would a solid model.

It is concluded that the laminar stagnation point approximation should be used in the predictive scheme with the turbulent calculation also being carried out to indicate an upper (extreme) limit on the convective heating process.

The discussion is also restricted to heat transfer under steady state conditions. It has been shown that for rates of change in velocity as they are usually encountered in aircraft the convective heat transfer may be regarded as quasi-steady. This means the heat transfer at each instant may be calculated with formulae valid for the steady state into which property values are introduced as they are encountered at this specific instant.

Laminar Stagnation Point Heat Transfer Coefficient

In the neighborhood of a stagnation point where the velocity distribution is given by $U_\delta = Cx$, the heat transfer coefficient is given by

$$h = A \ k\sqrt{\frac{C}{\nu}} \tag{21}$$

if the heat generation due to compressive work and viscous dissipation is neglected. The values of A given by Goldstein (15) depend upon the Prandtl number, Pr. A few values of A are listed in Table I.

Table I. The constant A for a circular cylinder
heat transfer coefficient

Pr	0.6	0.7	0.8	0.9	1.0	1.1
A	0.466	0.495	0.521	0.546	0.570	0.592

For a circular cylinder $U_\delta(x) = 2U_\infty \sin(x/\frac{1}{2}D)$ and, therefore, $C = (dU_\delta/dx)_{x=0} = 4U_\infty/D$ in the neighborhood of the stagnation point. Consequently the Nusselt number based on the diameter of the cylinder becomes

$$Nu = 2A\sqrt{\frac{U_\infty D}{\nu}} \tag{22}$$

Combined Analysis for the Heat Transfer Coefficient

Referring to Figure 2 and Equation (22), the principal problem is to calculate the equivalent approach flow velocity U_ω for the isolated, infinite cylinder.

By continuity

$$\rho_3 v_3 A_3 = \rho^* a^* A^* \tag{23}$$

The geometric porosity is defined as

$$P = A^*/A_{total} \tag{24}$$

and Equation (23) is written as

$$\frac{\rho_3 v_3}{\rho^* a^*} = \frac{A^*}{A_{total}} \cdot \frac{A_{total}}{A_3} = P \frac{A_{total}}{A_3}$$

The geometric factor A_{total}/A_3 is determined from the parachute cross section. We consider the flow entering the area A_3 to originate in a fictitious reservoir where the temperature is T_0, pressure p'_0, and density ρ'_0.

33

Since

$$\rho^* a^* = \frac{\rho^*}{\rho_0'} \ \rho_0' \ \sqrt{\gamma R T^*} = \frac{\rho^*}{\rho_0'} \sqrt{\frac{T^*}{T_0}} \ \sqrt{\gamma R} \ \rho_0' \ \sqrt{T_o} \qquad (25)$$

We shall assume, for the purpose of the heat transfer calculation only, that $\rho_3 \simeq \rho_0'$. This will prove to be conservative as far as surface temperatures are concerned.

Equations (24) and (25) are combined to yield

$$\frac{\rho^* a^*}{\rho_3 v_3} = \left[\frac{\rho^*}{\rho_0'} \sqrt{\frac{T^*}{T_0}} \ \sqrt{\gamma R} \right] \frac{\sqrt{T_0}}{v_3} = \frac{1}{P} \frac{A_3}{A_{total}} \qquad (26)$$

The velocity v_3 is taken to represent the approach flow velocity U_∞ required in the laminar stagnation point analysis. Equation (26) is rewritten

$$U_\infty = v_3 = \left(P \ \frac{A_{total}}{A_3} \right) \left[\frac{\rho^*}{\rho_0'} \sqrt{\frac{T^*}{T_0}} \ \sqrt{\gamma R} \right] \sqrt{T_0} \qquad (27)$$

Referring to Figure 9, the porosity P is given by

$$P = \frac{A^*}{A_{total}} = \frac{L^2}{(L + D)^2} \qquad (28)$$

where L is the distance between the filaments and D is the diameter of any filament. Therefore the expression for the approach velocity becomes

$$U_\infty = \left(\frac{L^2}{(L + D)^2} \right) \left(\frac{A_{total}}{A_3} \right) \left[\frac{\rho^*}{\rho_0'} \sqrt{\frac{T^*}{T_0}} \ \sqrt{\gamma R} \right] \sqrt{T_0} \qquad (29)$$

34
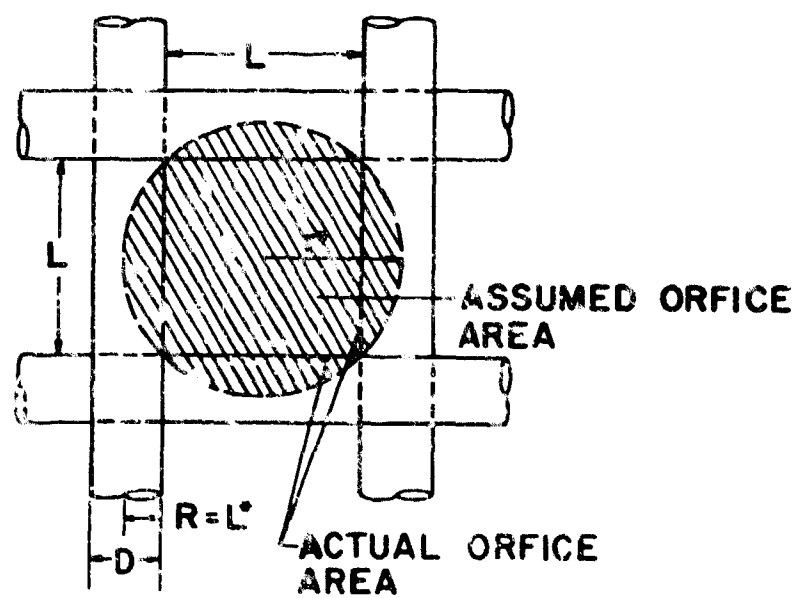
Figure 9. Typical Root Nozzle Geometry

For a Prandtl number of 0.71, the Goldstein result (Equation [22]) for the heat transfer coefficient to an infinite cylinder is

$$h = \frac{0.496}{Pr} \; c_{p_r} \; \sqrt{\rho_r \mu_r} \; \sqrt{\frac{2U_\infty}{1/2D}} \tag{30}$$

Now with $p'_0 = \rho'_0 R T_0$, $P_{ref} = \rho_{ref} R T_{ref}$, $P_{ref} = p'_0$ because of the condition of a constant static pressure across the stagnation point boundary layer,

$$\sqrt{\rho_r \mu_r} = \sqrt{\frac{p'_0 \mu_0}{RT_0}} \; \sqrt{\frac{T_0}{T_r} \cdot \frac{\mu_r}{\mu_0}} \tag{31}$$

If we make the relatively common assumption that $\mu = CT$, that is

$$\frac{\mu_r}{\mu_0} = \frac{T_r}{T_0} \tag{32}$$

the expression for the heat transfer coefficient becomes

$$h = \frac{(0.496) \; 2}{Pr} \underbrace{\left[\frac{\rho^*}{\rho'_0} \sqrt{\frac{T^*}{T_0}} \sqrt{\frac{\gamma}{R}} \right]^{1/2}}_{\substack{\text{sonic throat}}} \underbrace{\left[\left(\frac{L}{L+D} \right) \frac{1}{\sqrt{D}} \sqrt{\frac{A_{total}}{A_3}} \right]}_{\substack{\text{geo- wire shape} \\ \text{metric size factor} \\ \text{weave}}} \underbrace{c_{p_r} \sqrt{\mu_0} \; \frac{(p'_0)^{1/2}}{(T_0)^{1/4}}}_{\substack{\text{trajectory} \\ \text{variables}}} \tag{33}$$

leading constant

The heat transfer results for a variety of geometries are unified through the use of the sonic Reynolds number Re*. With the aid of equation (25),

36

$$Re^* = \rho^* c^* \frac{D}{\mu^*} = \left[\frac{\rho^*}{\rho_0'} \sqrt{\frac{T_0}{T^*}} \sqrt{\frac{\gamma}{R}} \right] \frac{D}{\mu_0} \frac{p_0'}{\sqrt{T_0}} \qquad (34)$$

and the final relation between h and Re* becomes

$$Nu^* = \frac{hD}{k} \approx 2(0.496) \left(\frac{L}{L+D} \right) \sqrt{\frac{A_3}{A_{total}}} \quad \sqrt{Re^*} \approx \left(\frac{L}{L+D} \right) \sqrt{\frac{A_3}{A_{total}}} \quad \sqrt{Re^*} \qquad (35)$$

Turbulent Analysis

Sibulkin [16] developed an approximate solution for the heat transfer to a constant-property, turbulent boundary layer with arbitrary freestream velocity and surface temperature distributions. In order to estimate rapidly the maximum rate of heat transfer which occurs near the throat of a supersonic nozzle, a throat approximation was developed which involves only the nozzle supply conditions, throat opening, and the throat radius of curvature. The Sibulkin prediction leads to the following relation for h:

$$h = \frac{C \, p_0 \left(\dfrac{\overline{\mu^*}}{\overline{\rho^*}} \right)^{1/5}}{(T_0)^{3/5} \, (r^* L^*)^{1/10}} \left(\frac{T_1}{\overline{T}} \right) \qquad (36)$$

where

h = heat transfer coefficient, $(BTU/sec\text{-}ft^2\text{-}{}^\circ R)$

C = axially symmetric constant, $(C = 0.0027 \ BTU/lb\text{-}sec^{4/5}\text{-}ft^{1/5}\text{-}{}^\circ R^{2/5})$

r* = nozzle throat radius, (ft)

L* = radius of curvature at nozzle throat, (ft)

37

p_0 = nozzle supply pressure, $(\text{lb}_f/\text{ft}^2)$

$\bar{\mu}*$ = dynamic viscosity at $\bar{T}$, (slugs/ft-sec)

$\rho*$ = sonic density at $\bar{T}$, (slugs/ft^3) = $(0.5283\ p_0)/(1716)(0.833\ T_0) \cdot T_0/\bar{T}$

T_0 = nozzle supply temperature, (°R)

$T*$ = sonic temperature = $0.833\ T_0$, (°R)

$\bar{T}$ = $(T_1^* + T_w)/2$, reference temperature, (°R)

The velocity gradient at the nozzle throat of an axisymmetrical-flow nozzle is

$$\left(\frac{dU_\delta}{dx}\right)^* = \left[\frac{2}{(\gamma + 1)}\right] \frac{1}{\sqrt{r*L*}} \ \sqrt{\gamma R T_0} \qquad (37)$$

The assumed circular nozzle throat of radius r* is frequently only an approximation to the actual rectangular geometry. That is, the orifice shown as the shaded area in Figure 9, $\pi r*^2$, is assumed to be circular with the same geometric area as the actual rectangular orifice, L^2. The corresponding stagnation point velocity gradient on an infinite, isolated cylinder, reduces to

$$\left.\frac{dU_\delta}{dx}\right)_{x=0} = \frac{2U_\infty}{R} = \left(\frac{2}{\gamma + 1}\right)^{\frac{\gamma - 3}{2(\gamma - 1)}} \frac{2}{L*}\left(1 + 2\sqrt{\pi}\ r*L* + \frac{L*^2}{\pi r*^2}\right)\sqrt{R T_0}$$

SECTION IV. INTERNAL ENERGY TRANSFER

The heat gained by a body is determined by the resistance to the
flow of heat at the surface as well as the internal resistance. Consider
a wall losing heat by convection to an ambient gas. At the wall, the
convective velocity is zero such that in the absence of radiation, the
energy transport is by conduction only. The Fourier conduction law
states that a rate of heat flow dQ in the direction of the normal n to
an area element dA is $dQ = - kdA \, \partial T/\partial n$. The minus sign indicates that
heat flows in the direction of decreasing temperature. According to the
Langmuir film concept the temperature gradient in the gas is confined to
a narrow layer of thickness δ. We simplify the convective heat exchange
process in the gas by assuming the entire thermal resistance to the heat
exchange between the wall and the gas is concentrated in a static film
which adheres to the wall, whereas outside this film all temperature
differences vanish as a result of the mixing motions of the gas. The
flow of heat to the wall is given by $Q_w = (k_g/\delta_g) \, A \, (T_g - T_w)$. Owing to
the difficulty in interpreting the film thickness δ_g, it is common en-
gineering practice to combine the quotient k_g/δ_g into a single quantity
designated h, the film heat transfer coefficient, and express the boun-
dary heat exchange as $Q = h \, A \, (T_g - T_w)$ where A is the boundary area in-
volved. The quantity hA is referred to as the surface conductance while
the value $1/hA = R_s$ is called the surface thermal resistance of the film
heat transfer process. For combined exchange processes the sum of the
individual resistances is the thermal resistance of the overall heat

transfer process. The dimensionless convective heat transfer coeffi-
cient is called the Nusselt number $Nu_{conv} = h\delta_g/k_g$ and assumes values both
greater than and less th.n the value of unity predicted by the oversim-
plified static film concept.

The heat entering the body is also governed by the Fourier conduction
law. Whenever the internal conduction is of importance, a dimensionless
conduction Nusselt number, given by $Nu_{cond} = h\delta_w/k_w = Bi$ (usually referred
to as the Biot number), enters as a parameter. The Biot number can be
thought of as the ratio of internal to surface resistance since

$$Bi = \frac{h\delta}{k} = \frac{\frac{\delta}{kA}}{\frac{1}{hA}} = \frac{R_i}{R_s} . \tag{38}$$

It is of primary importance to estimate the value of the Biot number in
a given problem in order to justify any further assumptions used to
simplify the analysis.

In any problem of transient heating (or cooling) the heat transfer
process is influenced by both the internal resistance R_i, and the surface
resistance R_s. The limiting cases are represented by a zero internal re-
sistance ($R_i = \delta/kA = 0 \rightarrow k \rightarrow \infty$; Newtonian heating or cooling) at one
extreme and a zero surface resistance ($R_s = 1/hA = 0 \rightarrow h \rightarrow \infty$) at the
other. The time increment in which equal temperatures are reached at two
different locations on the object is called the "transfer lag." In
Newtonian heating the transfer lag is zero.

Case A -- $R_i = 0$, Negligible Internal Resistance

When the body is constructed of material possessing a large thermal conductivity, its internal thermal resistance may be ignored so that the heat transfer process is controlled only by the surface resistance. No temperature differences can exist in the body under these conditions---the body is isothermal. Consider a body having an initial temperature T_i at $\tau = 0$ that is suddenly exposed to a fluid at temperature T_f. The rate of energy transfer from the surroundings for $\tau > 0$ is given by

$$Q = \rho_m V_m c_{p_m} \frac{dT}{d\tau} = hA \ (T_f - \overline{T}) \qquad (39)$$

where c_{p_m}, ρ_m, V_m, and A are the specific heat capacity, density, object volume, and object surface area, while $\overline{T} = \overline{T}(\tau) = \overline{T}_w (\tau)$ is the uniform temperature at any time τ and h and T_f are the heat transfer coefficient and ambient fluid temperature. We shall eliminate the bars for convenience. If h and T_f are independent of τ, Equation (39) integrates to yield

$$\frac{T - T_f}{T_i - T_f} = e^{-\left(\frac{hA}{\rho_m c_{p_m} V_m}\right)\tau} \qquad (40)$$

and the uniform temperature of the object rises exponentially with time. If we introduce the Biot number Bi and Fourier number Fo defined by the relations

$$Bi = \frac{h\delta_w}{k_w} \ , \qquad\qquad Fo = \frac{k_w \tau}{\rho_m c_{p_m} \delta_w^2} \qquad (41)$$

41
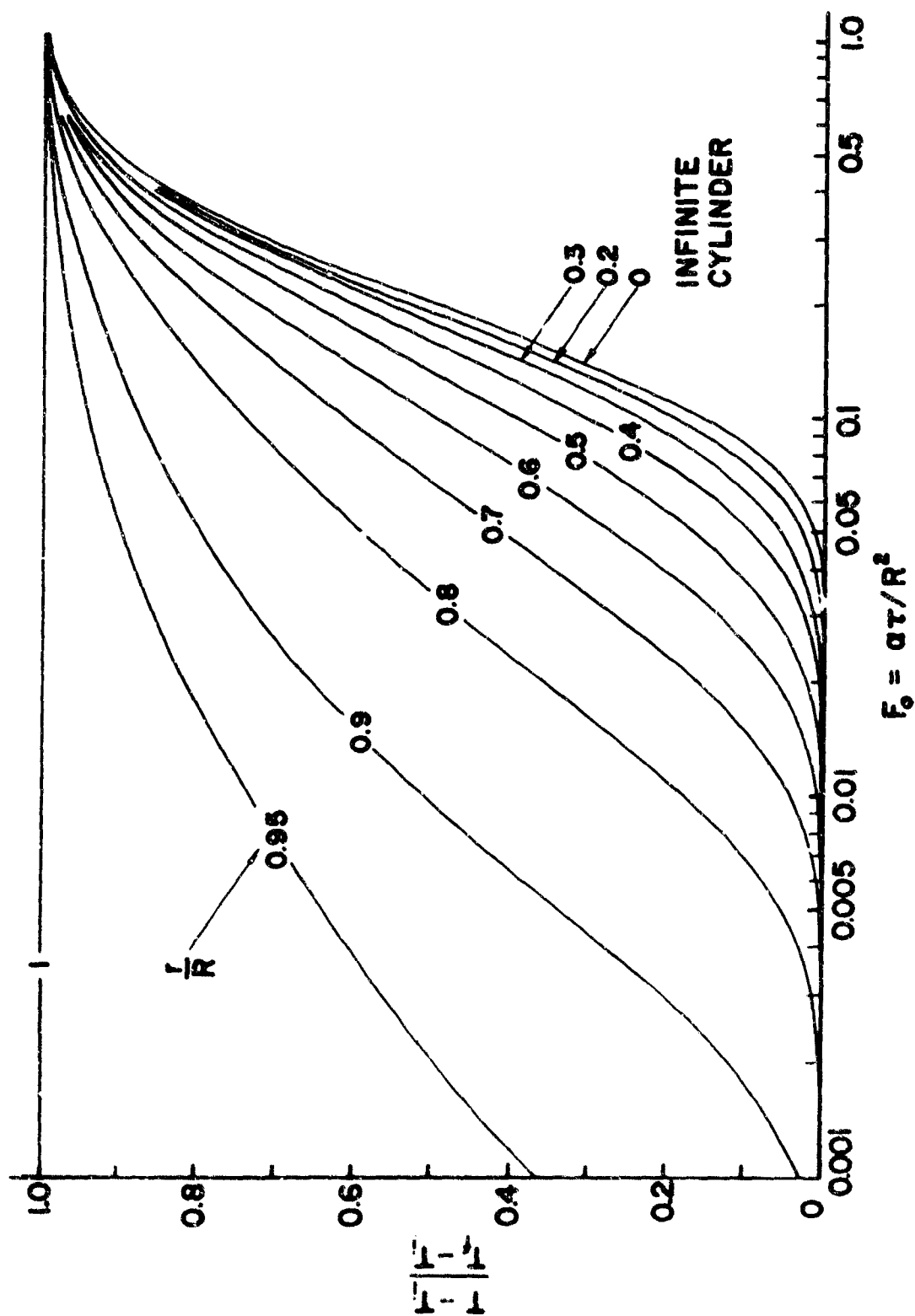
Figure 10. Temperature Response of a Cylinder, $0 \leq r \leq R$, After Sudden Change in External Surface Temperature at $r = R$ from t_i when $t = 0$ to t_f for $t > 0$ (Reference 20)
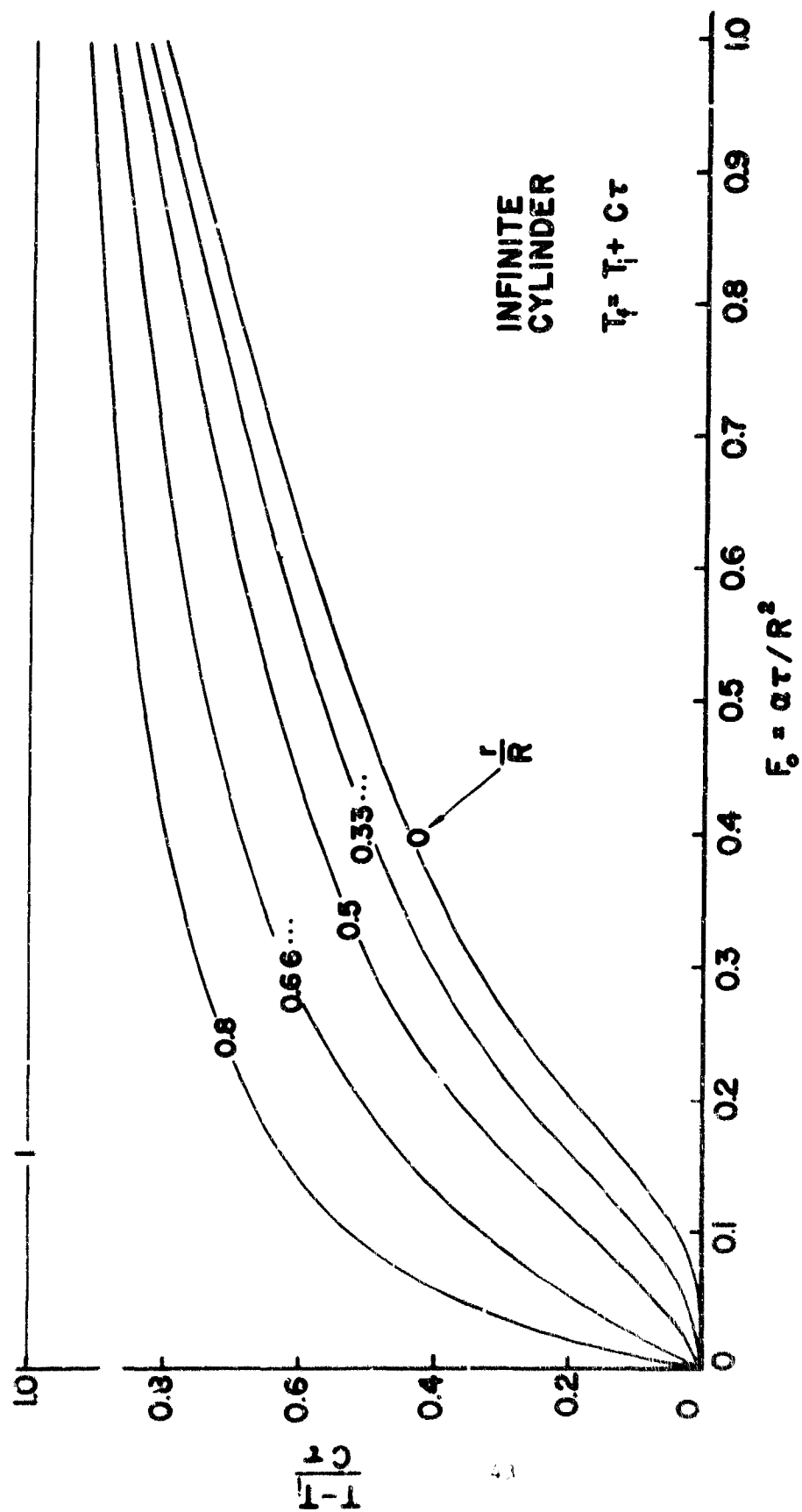
Figure 11. Temperature Response of a Cylinder, $0 \leq r \leq R$, with an External Surface Temperature at $r = R$ Varying Linearly with Time (Reference 20)
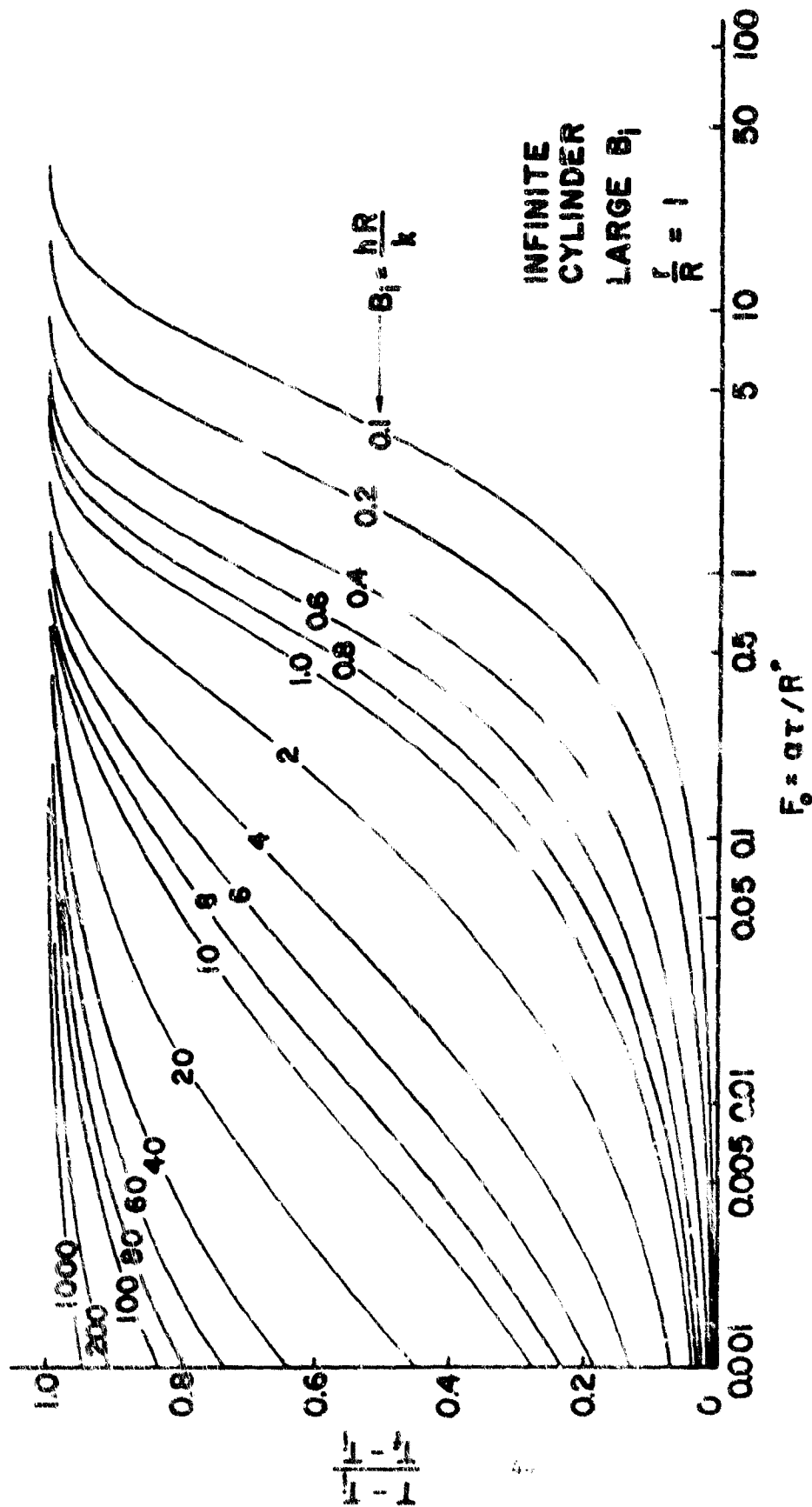
Figure 28. Temperature Response of a Cylinder, $0 \le r \le R$, After Sudden Exposure to a Uniform Temperature Convective Environment t_f at $r = R$; High B_i; (d)$r/R = 1$ (Reference 20)
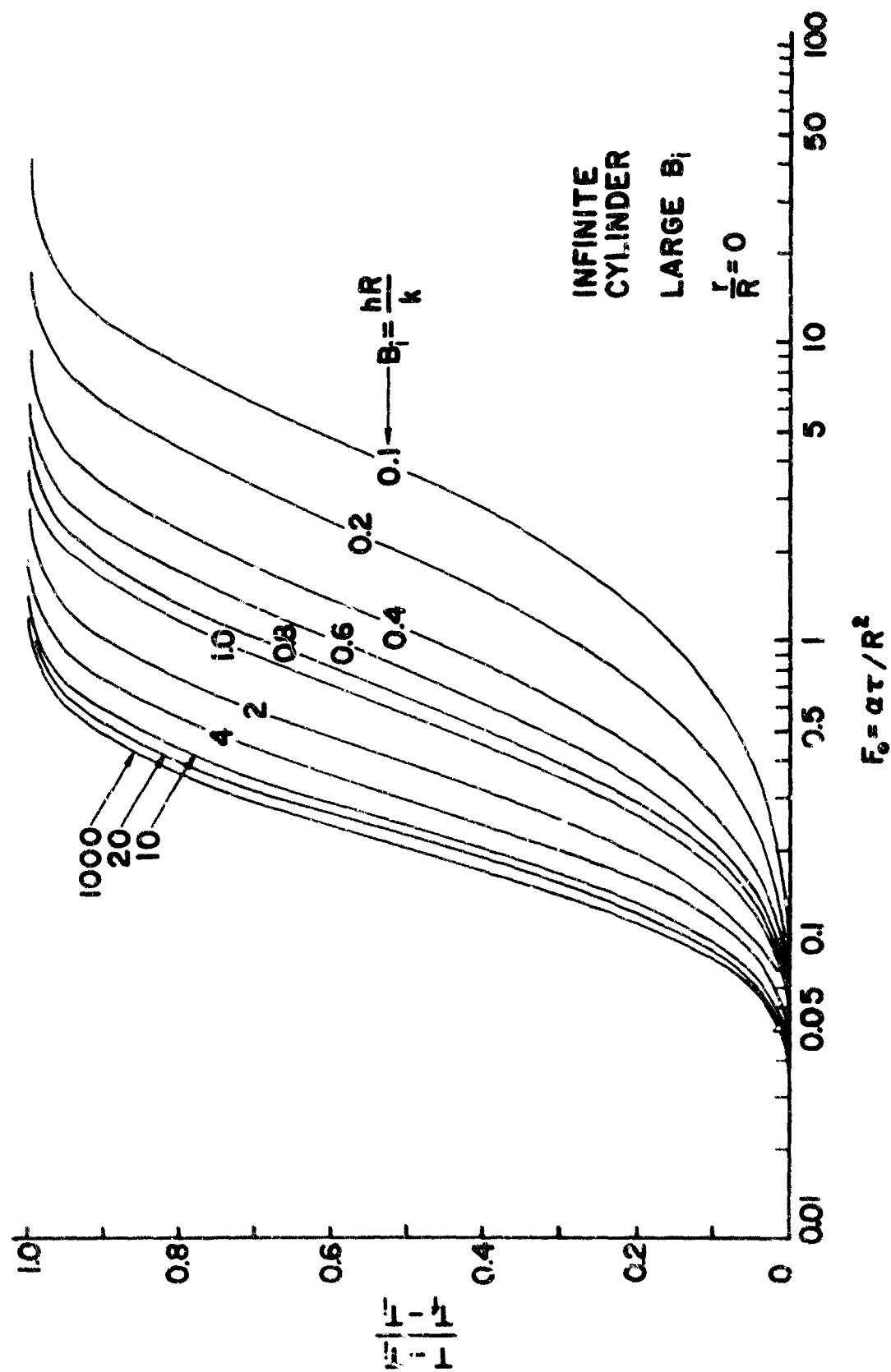
Figure 12. (Continued)
(Reference 20)

45

Figure 15. Temperature Response of a Cylinder, $0 \le r \le R$, After Sudden Exposure to a Uniform-Temperature Convective Environment T_f at $r = R$; Low Bi; (a) $r/R = 1$ (Reference 20)
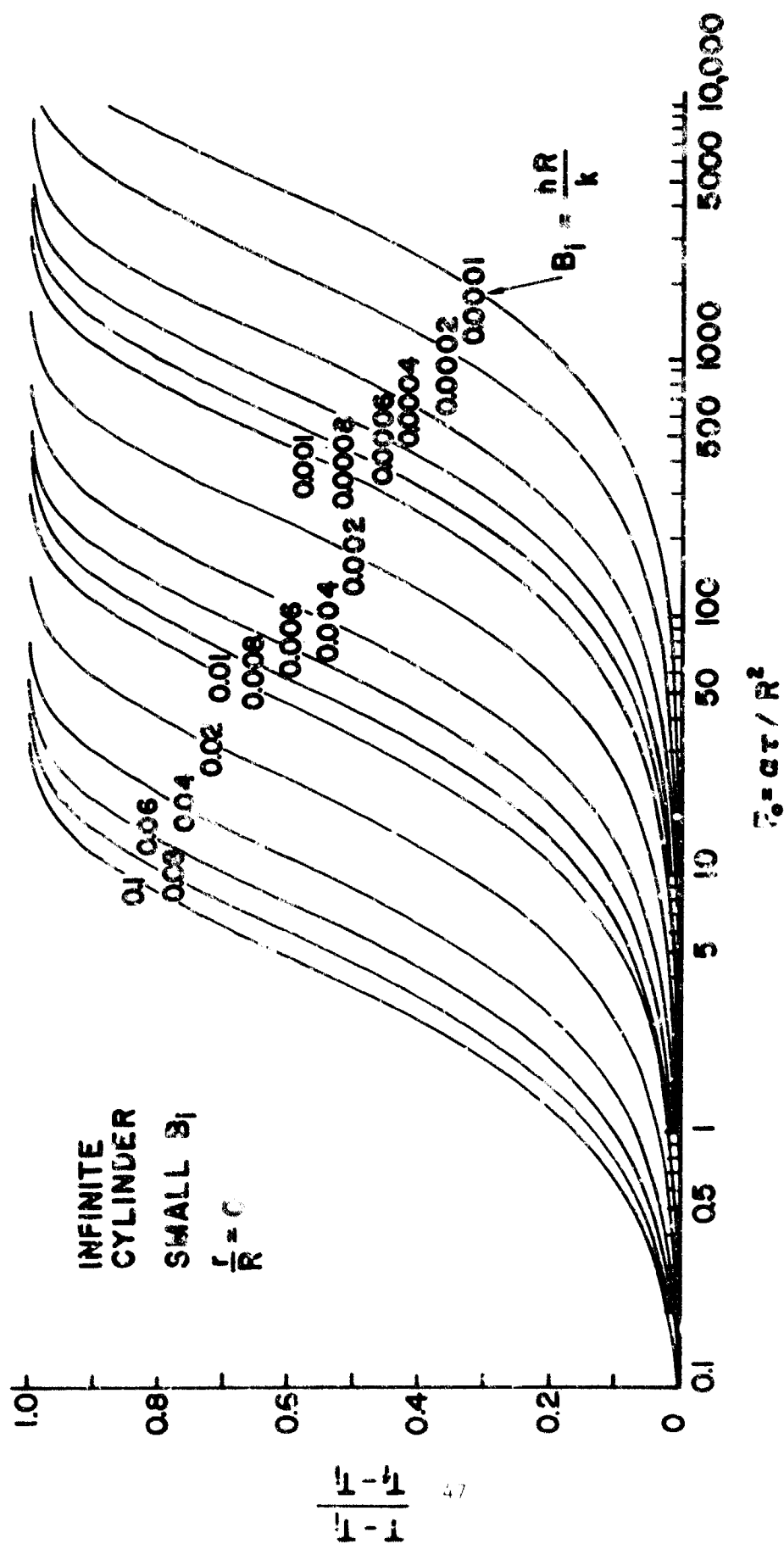
Figure 13. (Continued)
(Reference 20)

47

Equation (40) becomes

$$\frac{T - T_f}{T_i - T_f} = e^{-\left(\frac{A\delta_w}{V}\right)BiFo} \tag{42}$$

The product BiFo is independent of the object thermal conductivity k_w. For infinite cylinders the geometric factor $(A\delta_w/V) = 2$ and Equation (42) is rewritten

$$\frac{T - T_f}{T_i - T_f} = e^{-\frac{2h\tau}{\rho_m c_{p_m} \delta_w}} \tag{43}$$

If the temperature of the external fluid varies linearly so that $T_f = T_{f_i} \pm C\ (\tau)$, the solution becomes

$$\frac{T - T_f \pm C\ \dfrac{\rho_m c_{p_m} \delta_w}{2h}}{T_i - T_f \pm C\ \dfrac{\rho_m c_{p_m} \delta_w}{2h}} = e^{-\frac{2h\tau}{\rho_m c_{p_m} \delta_w}} \tag{44}$$

If the fluid temperature diminishes exponentially so that $T_f = T_{f_i} e^{-C\tau}$ the solution becomes (17)

$$\frac{(T - T_f) - T_{f_i}\ (\rho - 1)}{(T_i - T_{f_i}) - T_{f_i}\ (\rho - 1)} = e^{-\frac{2h\tau}{\rho_m c_{p_m} \delta_w}} \tag{45}$$

48

where

$$\rho = \frac{-1}{1 - \dfrac{\rho_m c_{p_m} \delta_w C}{2h}} \tag{46}$$

If the temperature of the external medium varies periodically (one-half cycle is an approximation to the atmospheric entry case) such that $T_f = \overline{T}_f + C \cos(\omega\tau)$, where $\overline{T}$ is the mean temperature of the fluid, constant with time, and S and ω are the amplitude and frequency of oscillation of the temperature difference $T_f - \overline{T}_f$, the solution is

$$\frac{T - \overline{T} - A'}{T_i - \overline{T} - A} = e^{-\dfrac{2h}{\rho_m c_{p_m} \delta_w} \tau} \tag{47}$$

where

$$A' = \rho C \left[\left(\frac{2h}{\rho_m c_{p_m} \delta_w} \right) \cos \omega\tau + \omega \sin \omega\tau \right] \tag{48}$$

$$A = \rho C \frac{1}{T} , \qquad \rho = \frac{\dfrac{2h}{\rho_m c_{p_m} \delta_w}}{\left(\dfrac{2h}{\rho_m c_{p_m} \delta_w} \right)^2 + \omega^2}$$

Case B -- $P_s = 0$, Negligible Surface Resistance

A class of problems exists in which the surface thermal resistance is negligible and the internal thermal resistance dominates the problem. If the ambient temperature of the surrounding fluid is $T_f(\tau)$ we take the temperature of the surface of the object to be $T_f(\tau)$ for $\tau > 0$.

a.) $\underline{T_f = \text{constant} \quad T_i = T_i(r)}$

Consider an infinitely long circular cylinder with the initial temperature distribution $T_i(r,0)$. The temperature of the surface $T(R,\tau)$ is suddenly changed to $T_f = \text{const}$ for all $\tau > 0$. The solution must satisfy the system

$$\frac{\partial^2 T}{\partial r^2} + \frac{1}{r} \frac{\partial T}{\partial r} = \frac{(\rho c_p)}{k} \frac{\partial T}{\partial \tau} = \frac{1}{\omega} \frac{\partial T}{\partial \tau} \tag{49}$$

$$T = T_i(r) \quad \text{at} \quad \tau = 0; \quad 0 \leq r \leq R$$
$$T = 0 \quad \text{at} \quad r = R; \quad \theta > 0 \tag{50}$$

For the special case of a uniform temperature distribution $T_i(r) = T_i$, the solution of the above system is

$$\frac{T - T_f}{T_i - T_f} = 2 \sum_{n=1}^{\infty} \frac{e^{-M_n^2 Fo}}{M_n} \frac{J_0\left(M_n \frac{r}{R}\right)}{J_1(M_n)} \tag{51}$$

where J_0 and J_1 are the zeroeth and first-order Bessel functions and M_n represents the roots of the zero-order Bessel function $J_0(M_n) = 0$.

The first five roots of $J_m(M_n)$ are given in the following table (18):

Table II. Roots M_n of $J_m(M_n) = 0$.

m	M_1	M_2	M_3	M_4	M_5
0	2.4048	5.5201	8.6537	11.7915	14.9309
1	3.8317	7.0156	10.1735	13.3237	16.4706

The series has been computed for the axial temperature history at the centerline $r = 0$ according to the following expansion:

$$\frac{T(0,\tau) - T_f}{T_i - T_f} = 2\left[\sum_{n=1}^{\infty} \frac{e^{-M_n^2 Fo}}{M_n J_1(M_n)}\right] = 2\left[\frac{e^{-M_1^2 Fo}}{M_1 J_1(M_1)} + \frac{e^{-M_2^2 Fo}}{M_2 J_1(M_2)} + \ldots\right] = C(Fo) \quad (52)$$

A few values of $C(Fo)$ are given in the following table:

Table III. Values of $C(Fo)$ in Equation (52)

Fo	C(Fo)	Fo	C(Fo)
0.020	0.99999	0.200	.50149
0.040	.99627	0.240	.39912
0.060	.97054	0.280	.21704
0.080	.91772	0.320	25167
0.100	.84836	0.360	.19973
0.120	.77293	0.400	.1585
0.140	.69798	0.500	.0887
0.160	.62692	1.000	.0049
0.180	.56126	1.500	.0003

b.) Transient Boundary Conditions $T_f = T_f(\tau)$, $\underline{T_i = \text{constant}}$

If the initial temperature of the cylinder is T_i and its surface temperature is $T_f(\tau)$ the solution is

$$T = T_i + 2\frac{\alpha}{R^2}\sum_{n=1}^{\infty}e^{-M_n Fo}\ M_n^2\ \frac{J_0\left(M_n\frac{r}{R}\right)}{J_1(M_n)}\int_0^\tau e^{\frac{\alpha M_n^2}{R^2}\lambda}\ T_f(\lambda)d\lambda \quad (53)$$

where $\alpha = k_w/\rho_w c_{p_w}$.

If the surface temperature undergoes a linear rise, we take $T_f(\tau) = T_i + C\tau$ where C is a constant time gradient in °F/hr, and the solution is

$$T - T_i = C\left(\tau - \frac{R^2 - r^2}{4\alpha}\right) + \frac{2CR^2}{\alpha}\sum_{n=1}^{\infty}e^{-M_n^2 Fo}\ \frac{J_0\left(M_n\frac{r}{R}\right)}{M_n^2 J_1(M_n)} \quad (54)$$

If the surface temperature undergoes a sinusoidal variation of the form $T = T_i[1 + \sin(\omega\tau + \epsilon)]$, then the solution is (19)

$$T - T_i = \frac{\phi_0\left(\sqrt{\frac{\omega}{\alpha}}\ r\right)}{\phi_0\left(\sqrt{\frac{\omega}{\alpha}}\ R\right)}\sin\left\{\omega\tau + \epsilon + \theta_0\left(\sqrt{\frac{\omega}{\alpha}}\ r\right) - \theta_0\left(\sqrt{\frac{\omega}{\alpha}}\ R\right)\right\}$$

$$+\frac{2\alpha}{R^2}\sum_{n=1}^{\infty}e^{-M_n^2 Fo}\ \frac{M_n\left(\omega\cos\epsilon - \alpha\frac{M_n^2}{R^2}\sin\epsilon\right)}{\left(\alpha^2\frac{M_n^4}{R^4} + \omega^2\right)}\ \frac{J_0\left(M_n\frac{r}{R}\right)}{J_1(M_n)}^+ \quad (55)$$

[+] For the notation $\phi_0(z)$ and $\theta_0(z)$ and some numerical values see McLochlan, _Bessel Functions for Engineers_, Oxford, 1934, p. 182.

52

Case C -- Finite Internal and Surface Resistance

The most general heat transfer problem involves heating or cooling of an object in which both the internal and surface resistance must be considered. Let the initial temperature throughout an infinitely long cylinder be T_i = constant. At the time $\tau = 0$ the cylinder is exposed to convective heating from an ambient fluid at T_f = constant. In addition the heat transfer coefficient is taken to be constant. The solution is

$$\frac{T - T_f}{T_i - T_f} = 2 \sum_{n=1}^{\infty} \frac{1}{M_n} \frac{J_1(M_n)}{\left[J_0^2(M_n) + J_1^2(M_n) \right]} e^{-M_n^2 Fo} J_0\left(M_n \frac{r}{R} \right) \qquad (56)$$

in which M_n are the roots of the eigenfunction Bessel equation

$$M_n \frac{J_1(M_n)}{J_0(M_n)} = Bi \qquad (57)$$

Note that the temperature-position solution is a function of two parameters ($Fo = \alpha\tau/R^2$, $Bi = hR/k$), rather than one as in the case of negligible surface resistance. The first three roots of Equation (57) are given in the following table:

Table IV. Roots of $M_1 J_1(M_n)/J_0(M_n) = Bi$

Bi	M_1	M_2	M_3
0	0.0000	3.8317	7.0156
0.02	0.1995	3.8369	7.0814
0.04	0.2814	3.8421	7.0213
0.10	0.4417	3.8577	7.0298

53

Bi	M_1	M_2	M_3
0.20	0.6170	3.8835	7.0440
0.40	0.8516	3.9344	7.0723
1.00	1.2558	4.0795	7.1558
5.00	1.9898	4.7131	7.6177
10.00	2.1795	5.0332	7.9569
100.00	2.3809	5.4652	8.5678

For values of Fo greater than 0.2, all terms in Equation (56) after the first become negligible. Therefore, for r equal to zero

$$\frac{T(0) - T_f}{T_i - T_f} = \frac{2J_1(M_1)e^{-M_1^2 Fo}}{M_1[J_0^2(M_1) + J_1^2(M_1)]} \tag{58}$$

With this approximation in mind, Heisler has presented time-temperature charts of the solution of Equation (56) for the range of Biot numbers from Bi = 0.01 to 100. The Heisler charts employ Equation (58) for the central temperature history $(J_0(0) = 1.0)$. It is clear that for any other position $0 < r \leq R$, $(T(r) - T_f)/(T_i - T_f) = (T(0) - T_f)/(T_i - T_f) \cdot J_0\left(M_1 \frac{r}{R}\right)$. A few useful values of the zeroeth and first-order Bessel functions of the first kind, $J_0(M)$ and $J_1(M_n)$, are

54

Table V.   Zeroeth and First-Order Bessel Functions

M_n	$J_0(M_n)$	$J_1(M_n)$
0.0	1.0000	0.0000
0.2	0.9900	0.0995
0.4	0.9604	0.1960
1.0	0.7652	0.4400
1.5	0.5118	0.5579
2.0	0.2239	0.5767
2.5	-0.0484	0.4971

It is clear that if $Bi < 0.1$, $M_1 < 0.5$ and $J_1(0.5\ r/R) > 0.95$.   It is seen that the temperature distribution through the cylinder is nearly uniform for $Bi < 0.1$.   Therefore, for $Bi < 0.1$ the combined heating process may be considered to be controlled by the surface resistance and the body uniform temperature is governed by the Newtonian equations.

For very large values of Biot number or for small values of the Fourier number the series solution given by Equation (56) converges slowly.   For this reason Heisler developed "short-time" charts for $1/Bi = 0.05$ to ∞ and $Fo = 0$ to 0.2.   For $Bi = 10$, $(T(R) - T_f)/(T_i - T_f)$ reaches the value 0.5 when $Fo = 0.01$.   In this case, the internal resistance prevents the passage of heat into the interior so that the surface layers must absorb the energy input.   The small mass available leads to   rapid temperature increases near the surface such that the negligible surface resistance case is approached in which the surface temperature instantaneously assumes the fluid temperature.

55

The asymptotic expansions for small values of time are cumbersome and are valid only if r/R is not small. Heisler computed the short-time curves for the cylinder surface while the other charts were obtained by "electrical analogy" on a "heat and mass flow analyzer." Charts for r/R = 0, 0.5, and 1.0 are presented as Figures 14 and 15.

Case D -- Approximate Methods

Of course the only method for solution of the general problem ($0 < Bi < \infty$) with variable boundary conditions [$h(\tau)$, $T_{aw}(\tau)$] involves numerical integration of the heat conduction equation. Short of this, it is often useful to obtain rapid estimates of the surface temperature, i.e., using the results of Sections IV. Case A and IV, Case B to predict the results of Section IV, Case C. Consider the two sketches below:

(a)

(b)

56
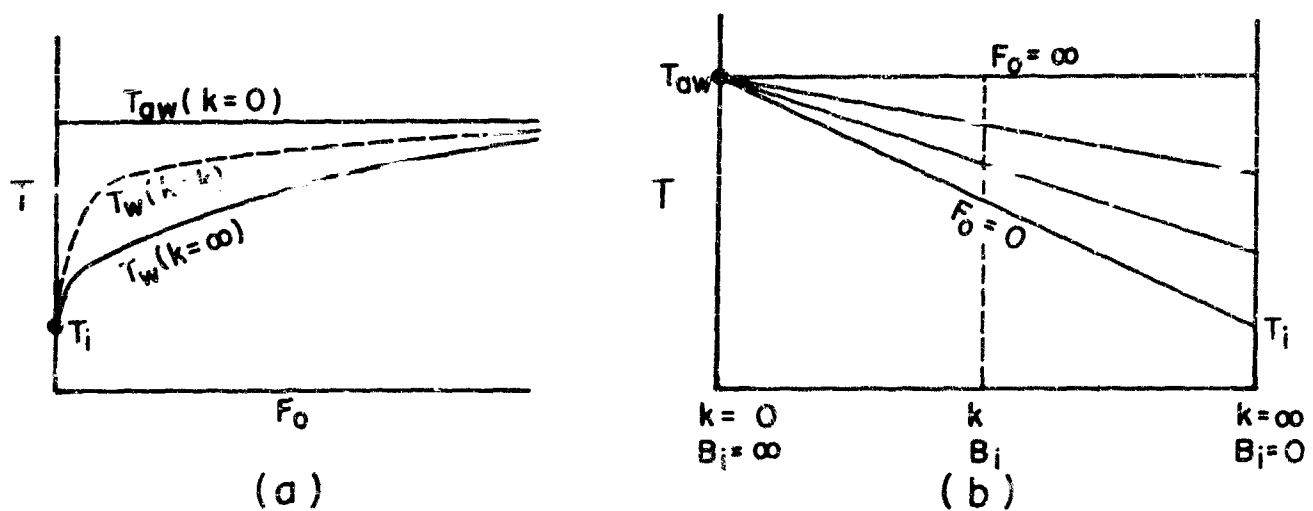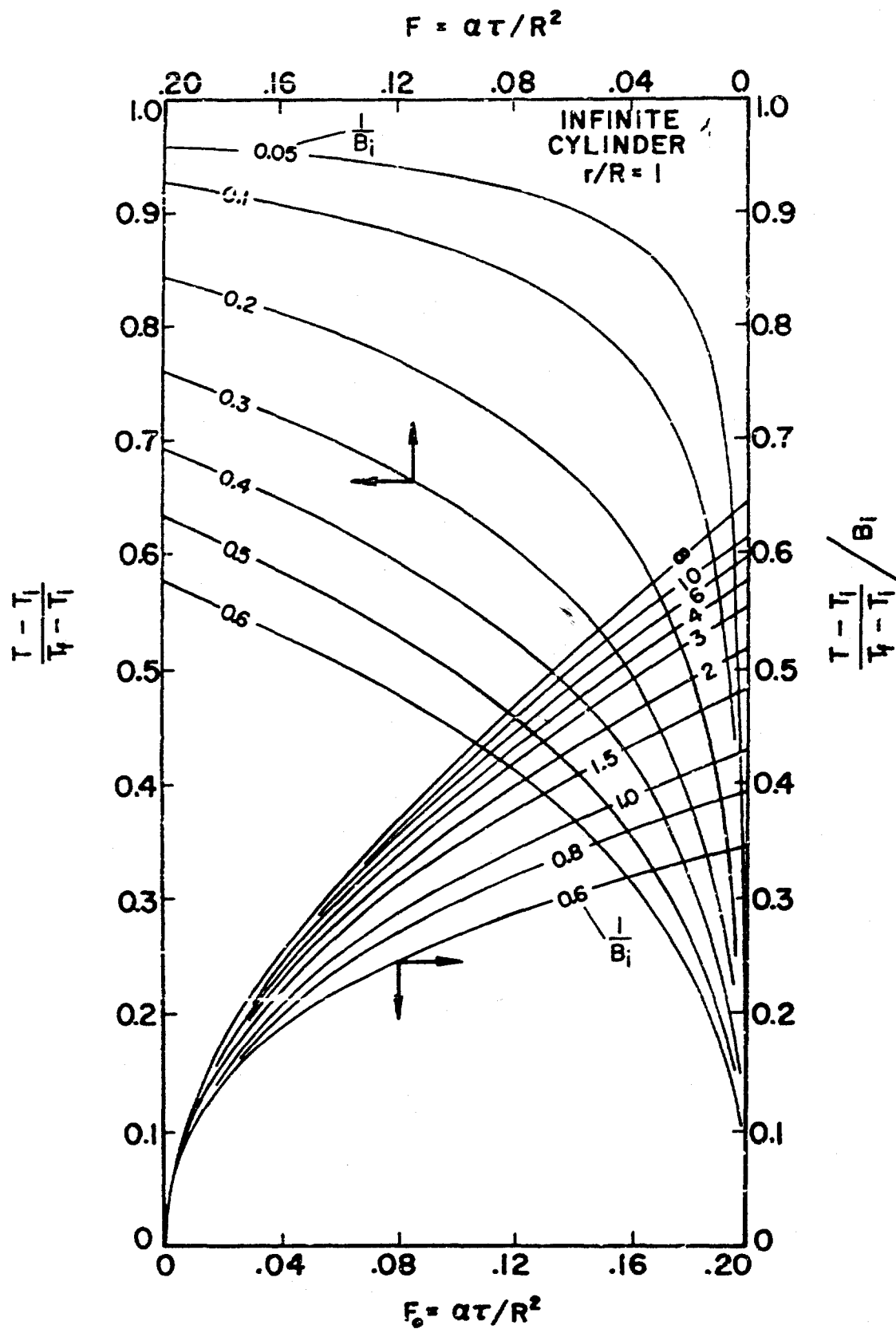
Figure 14. Chart for Determining Temperature History at Surface of Infinitely Long Cylinder (Reference 21)
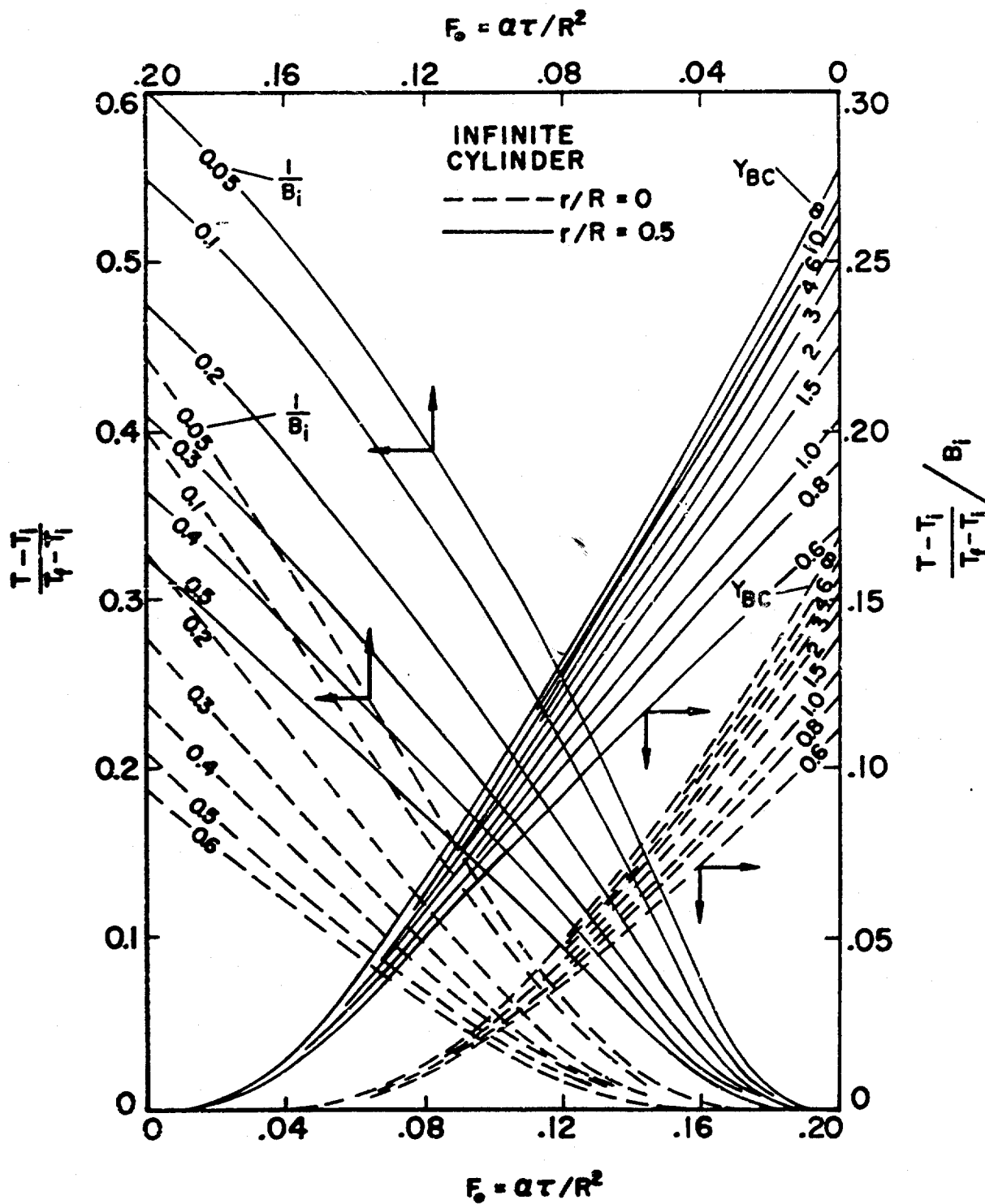
57

Figure ... ... at center ... ... infinitely long cylinder ... ...

The problem is to predict the intermediate Bi behavior from the limiting cases as is illustrated by the dashed lines in the sketches above. Asymptotic expansions in the two ranges Bi >> 0, Bi ≈ 0 are reasonable. A somewhat more useful, though cruder, approximation is the following:

$$\frac{T_{Bi} - T_{Bi=0}}{T_{Bi=\infty} - T_{Bi=0}} = \tanh \frac{\sqrt{Bi}}{C}$$

where C is an arbitrary constant. The hyperbolic tangent was chosen because it has the proper asymptotic behavior ($\tanh 0 = 0$, $\tanh \infty = 1$). Below is a short table of the hyperbolic tangent.

Table VI. Table of Tanh x

x	tanh x	x	tanh x
0	.0000	1.2	.8337
0.2	.1974	1.4	.8854
0.4	.3800	2.0	.9640
0.6	.5370	3.0	.9951
0.8	.6644	4.0	.9993
1.0	.7617	5.0	.9999

(If x > 5, tanh x = 1.0000 to four decimal places.)

A sample calculation may be carried out using the Heisler charts (Figures 16 and 17). For Fo = 0.2, Figure 16 reveals the following data:

Bi	$\dfrac{T(R) - T_i}{T_g - T_i}$	$\tanh(\sqrt{Bi}/2)$
∞	1.00	1.00
10	0.92	0.92
5	0.84	0.81
1.00	0.43	0.46
.50	0.26	0.33
.10	0.06	0.13
0	0	0

The approximation is examined for C = 2 above and is reasonable in the range $0.5 \leq Bi \leq 10$. This is the useful range of most parachute materials.

Figure 16. Heisler Chart for Determining Temperature History at Center of Infinitely Long Cylinder with Surface Resistance
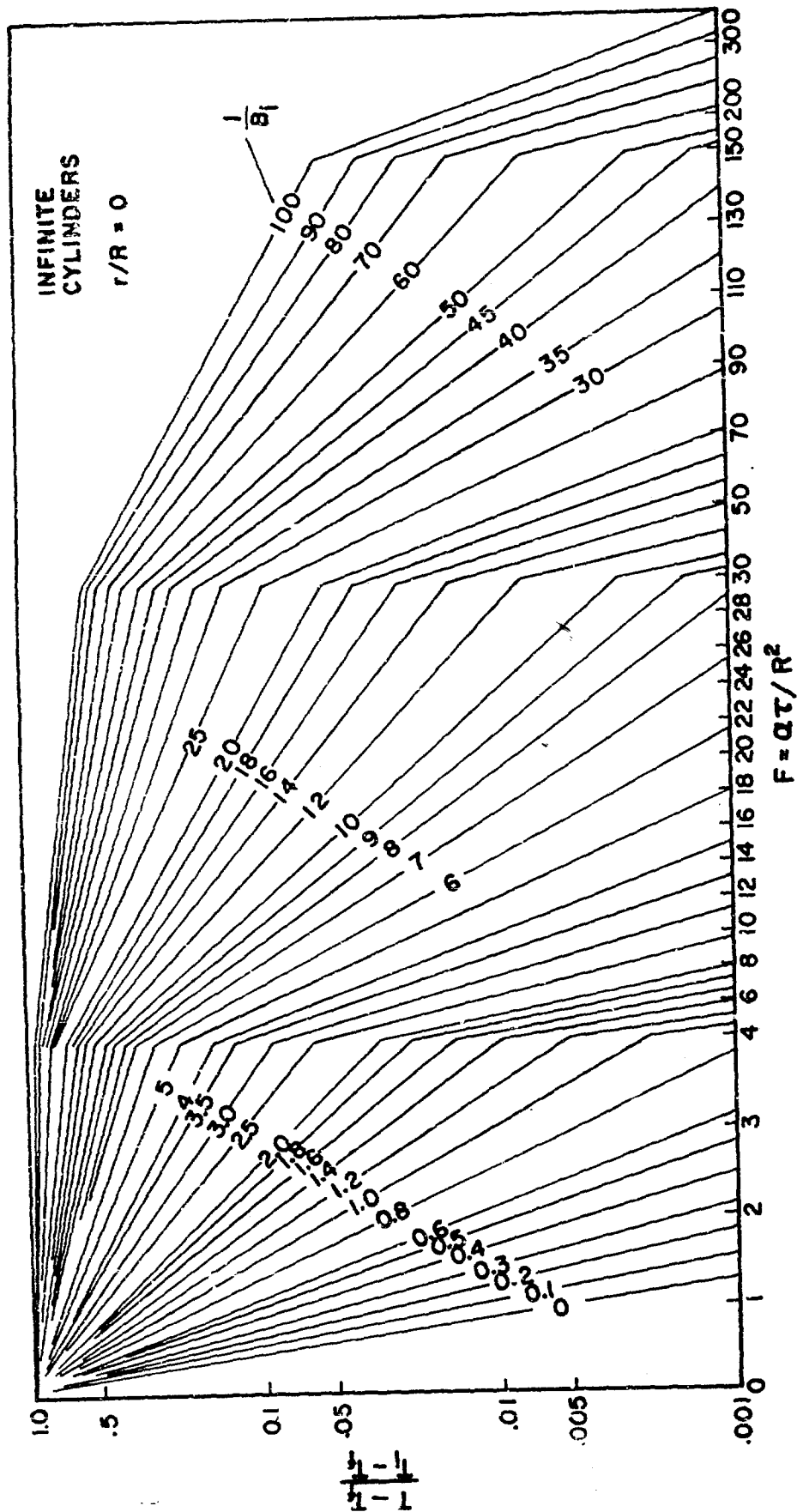
61
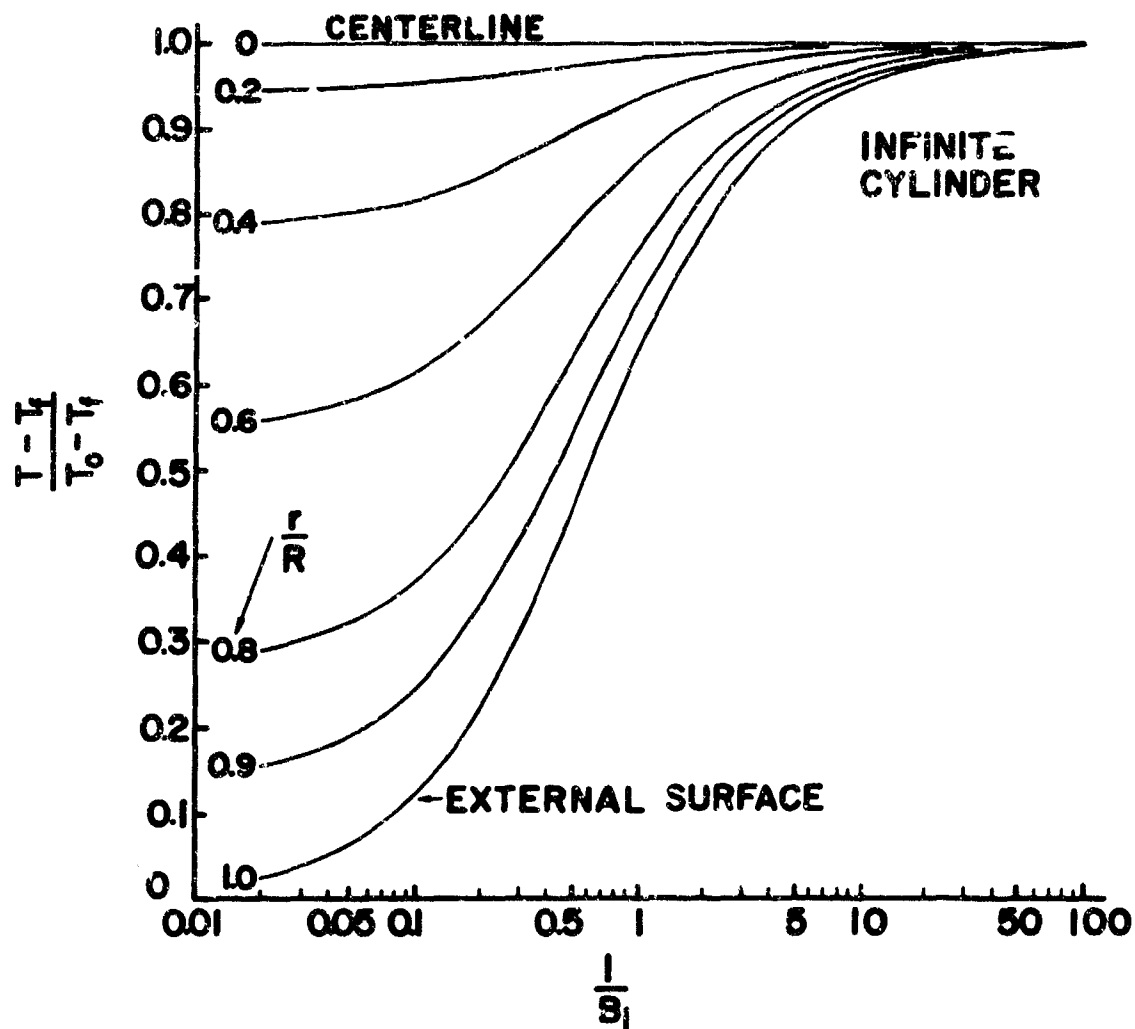
Figure 17. Heisler Position Correction Factors for Dimensionless
Temperature Ratios for Infinitely Long Cylinder.
To be Used with Figure 16 (Reference 21)

62

APPENDIX I.

APPLICATION OF THE PROPOSED

TECHNIQUES TO A PRACTICAL EXAMPLE

The analytical tools developed in the text were applied to a para-
chute which was launched by the Goodyear Corp. (22). The heat transfer
calculations are based on measured values of velocity versus altitude
(Figure 35 in Ref. 22) and calculated values of the Mach number, total
pressure, and total temperature. The important aerothermodynamic vari-
ables are tabulated in Tables VII and VIII. The data required for the
calculation of the convective heat transfer coefficients (Equations [33]
and [35]) are presented as the last two columns on the right in Table VIII.
These data are plotted in Figures 18 through 20. It is observed that
the parachute was deployed during the ascent phase of the trajectory.

Experimentally (23) it has been found that the actual pressure behind
the normal shock is less than p_0' calculated using normal shock theory in
the absence of any forebody wake. The ratio $p_0'_{actual} \big/ p_0'_{calculated}$ is
given in Reference 23 for two Mach numbers, i.e.,

$$M_1 = 3 \qquad\qquad p_0'_{act} \big/ p_0'_{calc} = 0.61$$

$$M_1 = 4 \qquad\qquad = 0.47$$

Since the present data fall in the range $4 \leq M_1 \leq 5.5$ extrapolation was
necessary. The following asymptotic behavior seems plausible:

$$M_1 \to 1 \qquad\qquad p_0'_{act} \big/ p_0'_{calc} \to 1$$

$$M_1 \to \infty \qquad\qquad \to 0$$

It is obvious to try the forms

$$\frac{P_0'{}_{act}}{P_0'{}_{calc}} = e^{B(M_1^2 - 1)} \qquad or \qquad e^{B(M_1 - 1)}$$

The best fit gave

$$\frac{P_0'{}_{act}}{P_0'{}_{calc}} = e^{\frac{M_1 - 1}{4}}$$

The general heat balance, Equation (14), was applied to one mesh, silently assuming that by rotation and fluctuation of the parachute the local variations in heating due to location on the parachute are leveled out.

From the given porosity $P = 0.13$ and the cross-section of one wire (see sketch below) one can calculate the mesh size to be $L = 0.578''$. From Figure 9 it is found that the total length of one thread is $L_{total} = 1.06\ L = 0.612''$. The perimeter of the wire is $Pe = 0.91''$. The total cross-section of an individual wire was found to be $A = 0.0507\ in^2$.

WIRE CROSS-SECTION
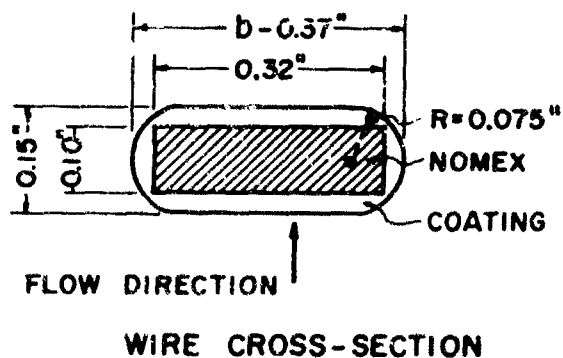
Since the element is composed of a layer of Nomex and a layer of D-65 coating, the average properties of the wire were found from

$$\left(\rho c_p\right)_{av} = \frac{(\rho c_p A)_{Nomex} + (\rho c_p A)_{D-65}}{A_{Nomex} + A_{D-65}} = 15.6 \frac{BTU}{ft^3 - {}^\circ R}$$

Finally, a crude correction to the calculated stagnation temperature has been made using a T_0 value 1000°R smaller than the one plotted in Figure 20. This corrected T_0 agrees more closely with the measured values reported in Reference 22.

The energy equation is applied in the following form:

$$V\rho c \frac{dT}{d\tau} = A_{conv} \cdot h(T_0 - T) + A_{rad} \Bigg[\alpha \cdot I$$

$$\times \epsilon\sigma \Bigg\{ \Big(F_{(p-sp)_1} T_{sp}^4 \quad F_{(p-ea)} \Big)(T_{ea}^4 - T^4)\Big(F_{(p-sp)_2}\Big)(T_{sp}^4 - T^4) \Bigg\} \Bigg]$$

where

Volume $\qquad V = 2 \cdot L_{tot} \cdot A$

Conv. Area $\qquad A_{conv} = 2 \cdot L_{tot} \cdot Pe$

Rad. Area $\qquad A_{rad} = 2 \cdot L \cdot h \qquad$ (projected area)

The shape factors are taken as the following (without further justi-fication):

$$\left. \begin{array}{l} F_{(p-sp)_1} = 2/3 \\ \\ F_{(p-ea)} = 1/3 \end{array} \right\} \qquad \text{outer surface}$$

65

$$F_{(p-sp)_1} = 1/2 \left.\right\} \quad \text{inner surface}$$

To compare better with the real stagnation temperature, a crude correction has been supplied by using a T_0 value 1000°R smaller than the one shown in Figure 5.

Figure 8 shows the plots for the eight cases
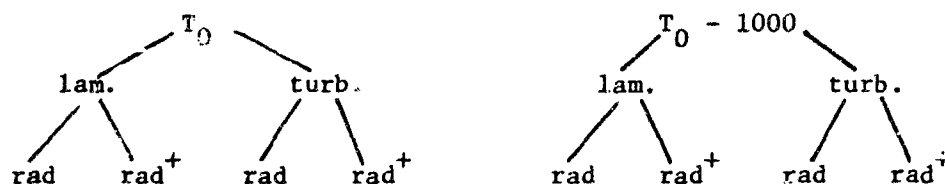
Abbreviations:

T = turbulent

L = laminar

R^+ = radiation increased

The radiation terms seem to have little influence for $\tau < 10$ sec and for the decreased stagnation temperature, where the change in the radiation term affects T only by less than 10°R. Comparison with the reported measurements indicates that only a more exact calculation, i.e., including conduction effects inside the wire, will give results in the vicinity of the available data.

Figure 18. Total Pressure Data for Goodyear Trajectory

Figure 19. Total Temperature Data for Goodyear Trajectory

Figure 20. Comparisons of Measured and Calculated Temperatures

LAMINAR
LAMINAR RAD. INCREASED
TURBULENT
TURBULENT RAD. INCREASED

TABLE VII

Data from Flight SP-5

Launching time 6:57:0.0

Given point: at 121,000 ft altitude   Mach 5.5

Launching Data

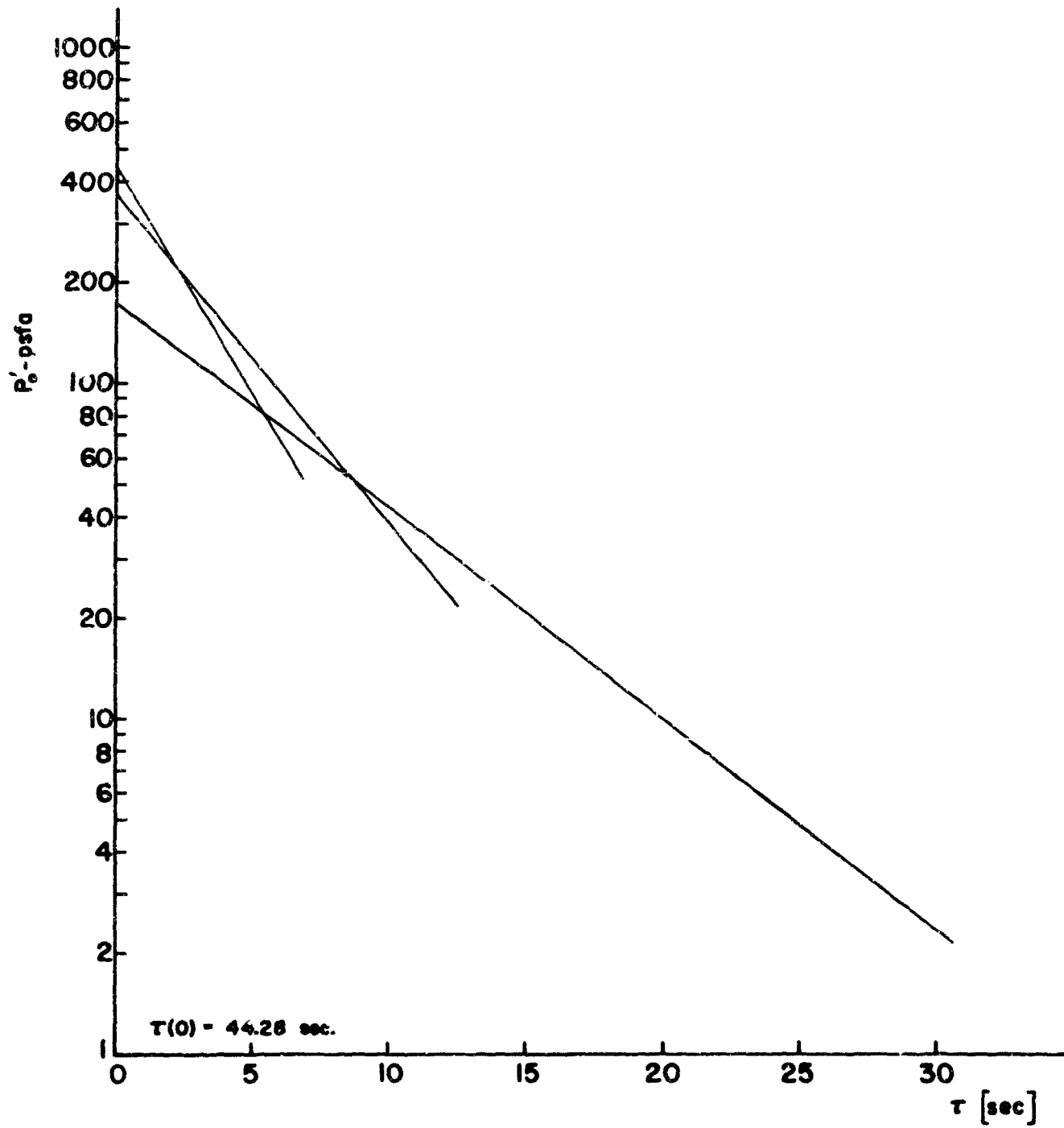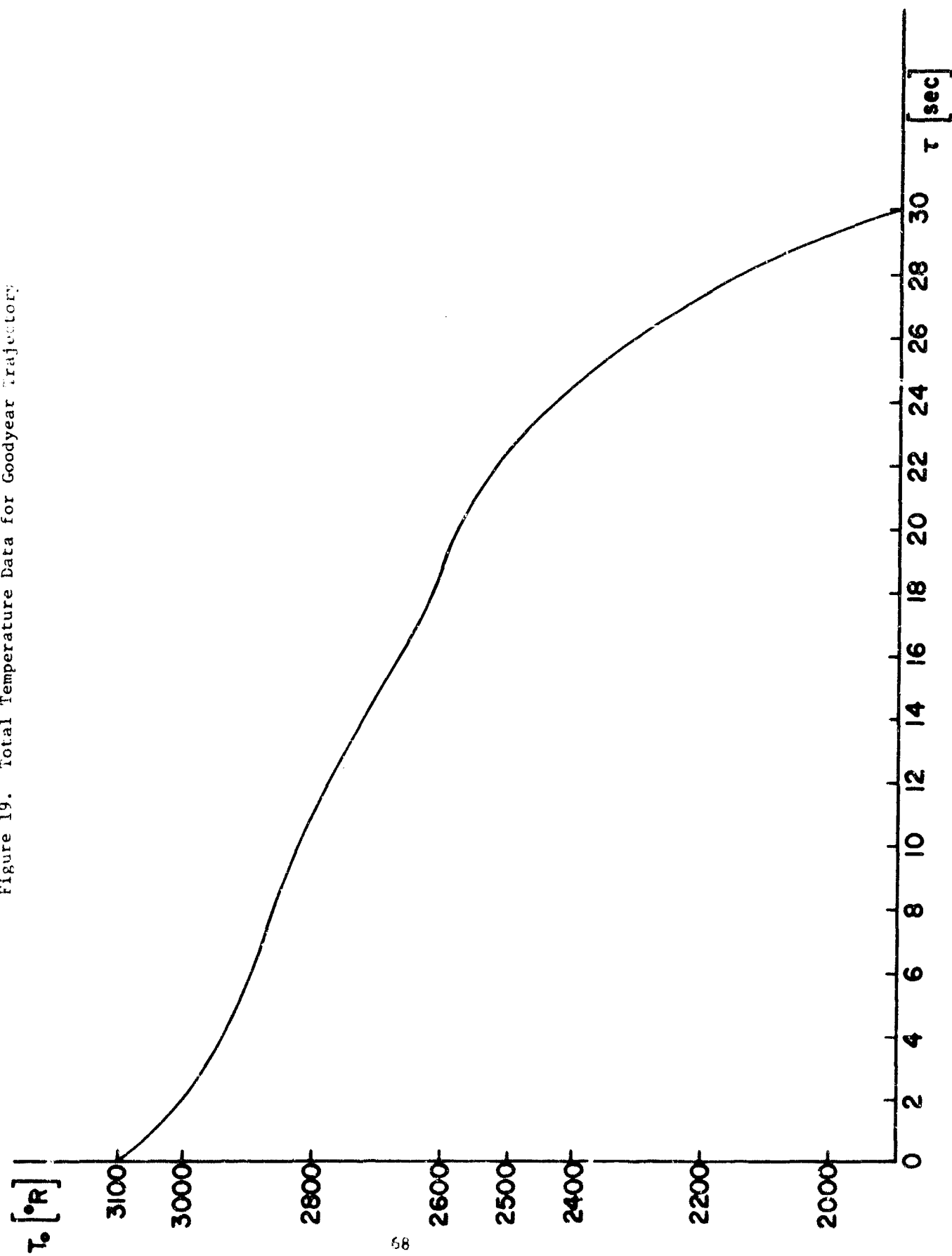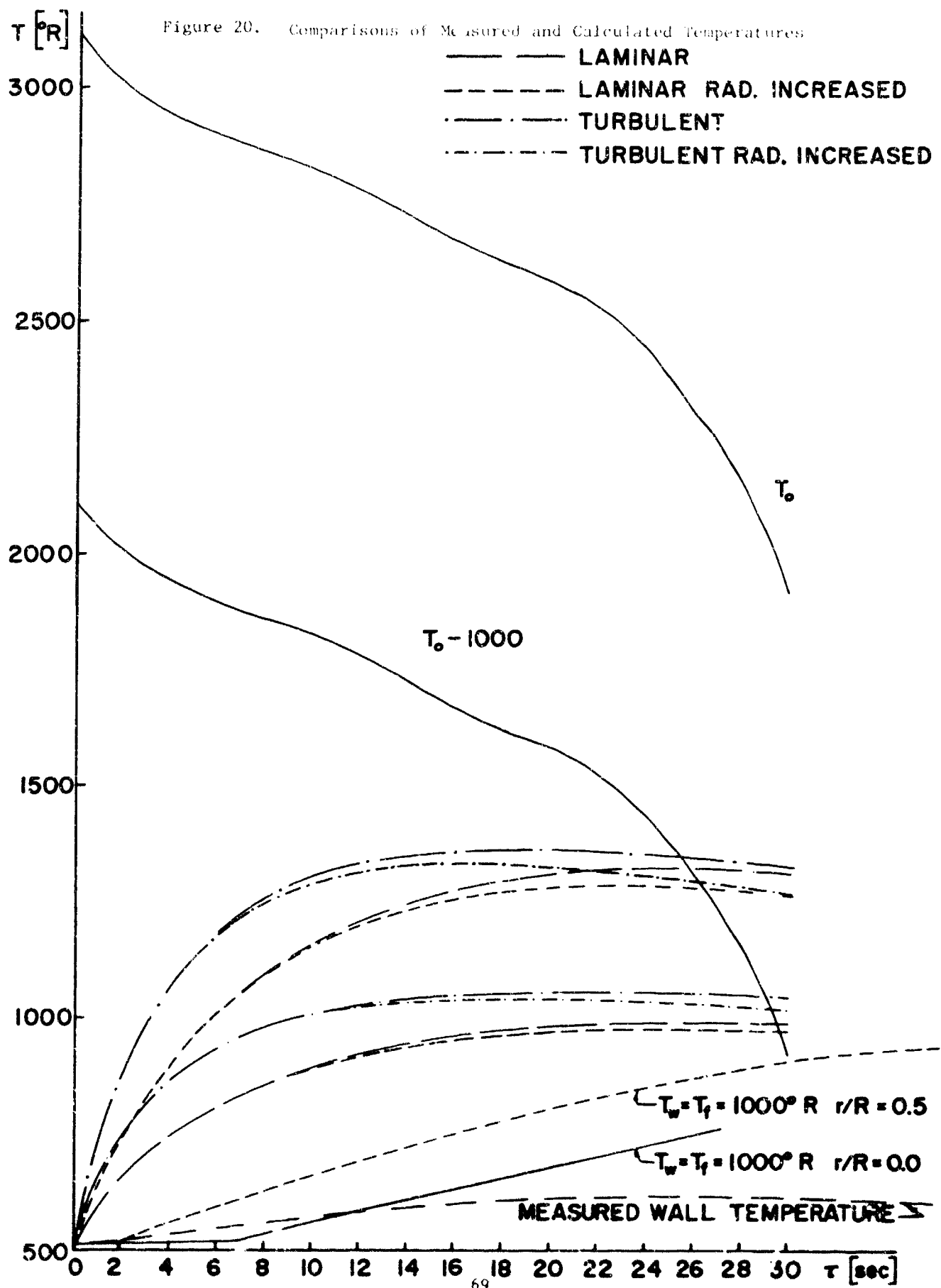| time [T + ... sec]	altitude [1000 ft]	V_1 [ft/sec]	a_1 [ft/sec]	M_1	p_1/p_0'	p_1 [atm]
44.28	118	5665	1038	5.458	0.02576	5.36×10^{-3}
45.28	123.1	5585	1063	5.254	0.02775	4.05×10^{-3}
46.28	128.2	5515	1088	5.069	0.02981	3.30×10^{-3}
47.28	133.3	5460	1112	4.910	0.03174	2.77×10^{-3}
48.28	138.4	5405	1136	4.758	0.03377	2.32×10^{-3}
49.28	143.5	5360	1161	4.617	0.03582	1.95×10^{-3}
50.28	148.6	5320	1186	4.486	0.03791	1.67×10^{-3}
51.28	154	5275	1207	4.370	0.03991	1.39×10^{-3}
52.28	159	5240	1227	4.271	0.04175	1.195×10^{-3}
53.28	164	5205	1238	4.204	0.04306	1.03×10^{-3}
54.28	169	5170	1244	4.156	0.04404	0.89×10^{-3}
55.28	173	5140	1247	4.122	0.04476	7.95×10^{-4}
56.28	179	5110	1248	4.095	0.04534	6.75×10^{-4}
57.28	184	5080	1248	4.071	0.04586	5.9×10^{-4}
58.28	189	5050	1247	4.050	0.04633	5.13×10^{-4}
59.28	193.9	5019	1243	4.038	0.04660	4.45×10^{-4}
60.28	198.8	4989	1238	4.030	0.04678	3.85×10^{-4}
61.28	203.5	4958	1232	4.024	0.04691	3.38×10^{-4}
62.28	208.4	4928	1222	4.033	0.04671	2.91×10^{-4}
63.28	213.4	4897	1209	4.050	0.04633	2.50×10^{-4}
64.28	218.1	4867	1196	4.069	0.04590	2.15×10^{-4}
65.28	222.8	4836	1182	4.091	0.04542	1.87×10^{-4}
66.28	227.4	4804	1166	4.120	0.04480	1.59×10^{-4}
67.28	232.1	4773	1148	4.158	0.04400	1.34×10^{-4}
68.28	236.8	4742	1128	4.204	0.04306	1.14×10^{-4}
69.28	241.5	4712	1105	4.264	0.04188	9.55×10^{-5}
70.28	246.0	4681	1077	4.346	0.04035	8.00×10^{-5}
71.28	250.3	4650	1047	4.441	0.03867	6.78×10^{-5}
72.28	254.6	4617	1017	4.540	0.03703	5.60×10^{-5}
73.28	258.9	4584	985	4.660	0.03518	4.55×10^{-5}
74.28	263.2	4553	965	4.720	0.03431	4.70×10^{-5}

70

TABLE VIII

Trajectory Parameters

time [sec]	M_{a_2}	T_3/T_2	T_2/T_1	T_0 [°R]	P_0' [lb_f/ft^2]
44.28	0.4094	1.0335	6.734	3113.15	440.5
45.28	0.4119	1.0339	6.307	3054.21	309.0
46.28	0.4142	1.0343	5.935	3005.57	234.35
47.28	0.4165	1.0347	5.626	2975.93	184.75
48.28	0.4189	1.0351	5.340	2943.15	145.44
49.28	0.4214	1.0355	5.083	2915.33	115.25
50.28	0.4238	1.0359	4.851	2892.80	93.257
51.28	0.4262	1.0363	4.651	2880.45	73.732
52.28	0.4283	1.0367	4.484	2870.14	60.594
53.28	0.4298	1.0369	4.373	2850.24	50.639
54.28	0.4310	1.0372	4.295	2824.26	42.782
55.28	0.4318	1.0373	4.240	2801.03	37.601
56.28	0.4325	1.0374	4.197	2780.73	31.517
57.28	0.4331	1.0375	4.159	2755.82	27.236
58.28	0.4336	1.0376	4.125	2725.85	23.441
59.28	0.4340	1.0377	4.107	2701.94	20.216
60.28	0.4342	1.0377	4.094	2675.04	17.423
61.28	0.4343	1.0377	4.068	2636.77	15.254
62.28	0.4341	1.0377	4.099	2629.20	13.189
63.28	0.4336	1.0376	4.125	2609.42	11.423
64.28	0.4331	1.0375	4.155	2587.79	9.9162
65.28	0.4326	1.0374	4.191	2560.75	8.7159
66.28	0.4319	1.0373	4.237	2524.28	7.5134
67.28	0.4311	1.0372	4.298	2486.00	6.4472
68.28	0.4298	1.0370	4.373	2440.73	5.6047
69.28	0.4285	1.0367	4.472	2378.43	4.8274
70.28	0.4267	1.0364	4.610	2313.51	4.1973
71.28	0.4247	1.0361	4.773	2225.48	3.7117
72.28	0.4228	1.0358	4.946	2148.70	3.2015
73.28	0.4206	1.0354	5.160	2062.89	2.7380
74.28	0.4196	1.0352	5.270	1914.96	2.28

REFERENCES

1. Hritzay, D., and Wiant, "Wire Cloth Structure for a Radiating Re-
    Entry Vehicle," AVCO-Everett Research Report 123, 1962.

2. Kyser, A. C., "The Rotornet: A High-Performance Hypersonic Decelera-
    tor for Planetary Entry," NASA CR-247, June 1965.

3. Scott, C. J., and Eckert, E. R. G., "Experiments on the Thermal Per-
    formance of Ribbon Parachutes," Air Force Flight Dynamics Laboratory
    Report AFFDL-TR-64-192, May 1965.

4. Edwards, R. C., et. al., "Study and Exploratory Free-Flight Investi-
    gation of Deployable Aerodynamic Decelerators Operating at High Alti-
    tudes and at High Mach Numbers,"FDL-TDR-64-35, July 1964.

5. Nebiker, F. R., "Aerodynamic Deployable Decelerator Performance-Evalu-
    ation Program," AFFDL-TR-65-27, August 1965.

6. Koh, J. C. Y., and Hartnett, J. P., "Measured Pressure Distribution
    and Local Heat Transfer Rates for Flow over Concave Hemispheres,"
    ARS Journal, Vol. 31, No. 1, January 1961.

7. Korst, H. H., Chow, W. L., and Zumwalt, G. W., "Research on Transonic
    and Supersonic Flow of a Real Fluid at Abrupt Increases in Cross
    Section (Final Report)," University of Illinois Eng. Exp. Station
    TR 392-5, December 1959.

8. Cornish, R. H., Ahimaz, F. J., Beadle, C. W., and Foster, K., "Mass
    Transfer Cooling of Parachute Materials," WADC-TR-58-684, September 1959.

9. Hermann, R., "Problems of Hypersonic Flight at the Re-Entry of Satellite
    Vehicles," University of Minnesota Rosemount Aeronautical Labora-
    tories RAL-RR-153, November 1958.

10. Eckert, E. R. G., Hartnett, J. F., and Turnacliff, R.D., "Transient
    Temperatures of Parachutes During Descent," WADC-TN-57-320, August 1957.

11. Eckert, E. R. G., "Survey on Heat Transfer at High Speeds," WADC-TR-54-
    70, April 1954.

12. Rose, P., Probstein, R., and Adams, M. S., "Turbulent Heat Transfer
    Through a Highly-Cooled, Partially Dissociated Boundary Layer," Journ.
    of Aero. Sciences Vol. 25, No. 12, December 1958.

13. Detra, R. W., and Hidalgo, H., "Generalized Heat Transfer Formulas
    and Graphs for Nose Cone Reentry into Atmosphere," Journ. American
    Rocket Society, Vol. 31, 1961.

14. Eckert, E. R. G., et al, "An Experimental Study of the Distribution of Convective Heat Transfer to a Large-Scale Model of Parachute Cloth," AFFDL-TR-66-13, May 1966.

15. Goldstein, S., Modern Developments in Fluid Dynamics, Vol. 2, Oxford University Press, N w York, 1938.

16. Sibulkin, M., "Heat Transfer to an Incompressible Turbulent Boundary Layer and Estimation of Heat Transfer Coefficients at Supersonic Nozzle Throats," J. Ae. Sciences, Vol. 23, No. 2, February 1956.

17. Kudryavtsev, Y. V., et al, Unsteady State Heat Transfer, Iliffe Books Ltd., London, 1966.

18. Schneider, P. J., Conduction Heat Transfer, Addison-Wesley Publishing Company, Inc., Reading, Mass., 1957.

19. Carslaw, H. S., and Jaeger, J. C., Conduction of Heat in Solids, Oxford University Press, 1950.

20. Schneider, P. J., Temperature Response Charts, John Wiley and Sons, Inc., New York, 1963.

21. Heisler, M. P., "Temperature Charts for Induction and Constant Temperature Heating," Trans. ASME, Vol. 69, April 1947.

22. Bloetscher, F., and Arnold, W. V., "Aerodynamic Deployable Decelerator Performance-Evaluation Program," AFFDL-TR-67-60, December 1967.

23. Noreen, R. A., and Hosker, R. P., "Pressure Distribution on Several Rigid Hyperflo Models at Mach 3.0 and 4.0, AFFDL-TR-67-84, June 1967.

DOCUMENT CONTROL DATA - R & D

(Security Classification of title, body of abstract and indexing annotation must be entered when the overall report is classified)

1. ORIGINATING ACTIVITY *(Corporate author)*	2a. REPORT SECURITY CLASSIFICATION
University of Minnesota Institute of Technology Mechanical Engineering Dept Minneapolis, Minnesota 55455	Unclassified
	2b. GROUP N/A

3. REPORT TITLE

The Prediction of Material Temperature on Woven Retardation Devices

4. DESCRIPTIVE NOTES *(Type of report and inclusive dates)*

Final Report   August 1966 - September 1967

5. AUTHOR(S) *(First name, middle initial, last name)*

Scott, Charles J

6. REPORT DATE	7a. TOTAL NO. OF PAGES	7b. NO OF REFS
	73	23

8a. CONTRACT OR GRANT NO. AF33615-67-C-1028	9a. ORIGINATOR'S REPORT NUMBER(S)
b. PROJECT NO. 6065	
c. Task No. 606505	University of Minnesota HTL-TR-71
	9b. OTHER REPORT NO(S) *(Any other numbers that may be assigned this report)*
d.	AFFDL-TR-67-170

10. DISTRIBUTION STATEMENT

This document is subject to special export controls and each transmittal to foreign governments or foreign nationals may be made only with prior approval of the AF Flight Dynamics Laboratory (FDFR), Wright-Patterson AFB, Ohio.

11. SUPPLEMENTARY NOTES	12. SPONSORING MILITARY ACTIVITY
N/A	AFFDL (FDFR) Wright-Patterson AFB, Ohio

13. ABSTRACT

The primary purpose of this report is to present analytical techniques for the pre-diction of instantaneous parachute temperatures for any prescribed flight condition and history of operation. Sample calculations are presented which illustrate the technique by comparing measured parachute temperature histories with several pre-dictive techniques. A variety of exact, transient heat conduction solutions are included (for a cylindrical geometry) which cover a range of trajectory possibilities. This was done because the transfer of heat to a conventional fabric or coated-fabric parachute is governed primarily by the large resistance to heat conduction into the interior. The commonly used infinite thermal conductivity case is shown to produce surface temperatures which fall considerably below the surface temperature predicted by more exact (complete) energy balances. For the extreme applied heat flux case (atmospheric entry), internal temperatures are accurately predicted by assuming the wall temperature instantaneously assumes a steady state, radiation equilibrium value ($q_w = 0$) and internal conduction governs the process. An approximate method is pre-sented for the calculation of parachute fabric temperatures when both the internal and external resistances to the flow of heat are of importance. The results are compared with flight test data on a full-scale parachute.

The distribution of this Abstract is unlimited.

DD FORM 1473

14 KEY WORDS	LINK A		LINK B		LINK C	
	ROLE	WT	ROLE	WT	ROLE	WT
Heat Transfer						
Supersonic Parachutes						
Analytical Temperature Predictions						
Aerodynamic Heating						